

NEURAL CONTROL OF PARAMETRIC SOLUTIONS FOR HIGH-DIMENSIONAL EVOLUTION PDES*

NATHAN GABY[†], XIAOJING YE[‡], AND HAOMIN ZHOU[§]

Abstract. We develop a novel computational framework to approximate solution operators of evolution partial differential equations (PDEs). By employing a general nonlinear reduced-order model, such as a deep neural network, to approximate the solution of a given PDE, we realize that the evolution of the model parameter is a control problem in the parameter space. Based on this observation, we propose to approximate the solution operator of the PDE by learning the control vector field in the parameter space. From any initial value, this control field can steer the parameter to generate a trajectory such that the corresponding reduced-order model solves the PDE. This allows for substantially reduced computational cost to solve the evolution PDE with arbitrary initial conditions. We also develop comprehensive error analysis for the proposed method when solving a large class of semilinear parabolic PDEs. Numerical experiments on different high-dimensional evolution PDEs with various initial conditions demonstrate the promising results of the proposed method.

1. Introduction. Partial differential equations (PDEs) are ubiquitous in modeling and are vital in numerous applications from finance, engineering, and science [23]. As the solutions of many PDEs lack analytical form, it is necessary to use numerical methods to approximate the solutions [4, 23]. Traditional numerical methods such as finite difference and finite element methods rely upon the discretization of problem domains, which does not scale to high-dimensional problems due to the so-called “curse of dimensionality”.

In recent years, a class of nonlinear reduced-order models, known as deep neural networks (DNNs), have emerged as powerful tools for solving high-dimensional PDEs [5, 16, 21, 30, 31, 33, 43, 69]. For example, in [5, 16, 21, 69, 85], the solution of a given PDE is parameterized as a DNN, and the network parameters are trained to minimize potential violations (in various definitions) to the PDE. These methods have shown numerous successes in solving a large variety of PDEs empirically. Their successes are partly due to the provable universal approximation power of DNNs [34, 49, 84]. On the other hand, these methods aim at solving specific instances of PDEs, and as a consequence, they need to start from scratch for the same PDE whenever the initial and/or boundary value changes.

There have also been recent studies to find solution operators of PDEs [47, 53]. These methods aim at finding the map from the problem’s parameters to the corresponding solution. Finding solution operators has substantial applications as the same PDE may need to run many times with different initial or boundary value configurations. However, existing methods fall short in tackling high-dimensional problems as many require spatial discretization to represent the solution operators using DNNs.

In this paper, we propose a new approach to find solution operators of high-dimensional evolution PDEs. For a given PDE, we first parameterize its solution as a general reduced-order model, such as a DNN, whose parameters denoted as θ are to be determined. Then we seek to find a vector field on the parameter space which describes how θ evolves in time. This vector field essentially acts as a controller on the parameter space, steering the parameters so that the induced DNN evolves and approximates the PDE solution for all time. Once such a vector field is found, we can easily change the initial conditions of the PDE by simply starting at a new point in the parameter space. Then we follow the control vector field to find the parameter trajectory which gives an approximation of the time-evolving solution. Thus, different initial conditions can be considered for the same PDE without solving it repeatedly. Our contributions can be summarized as follows.

1. We develop a new computational framework to find the solution operator of any given initial value problem (IVP) defined by high-dimensional nonlinear evolution PDEs. This framework is purely based on the evolution PDE itself and does not require any solutions of the PDE for training. Once we find the solution operator, we can quickly compute solutions of the PDE with any initial value at a low computational cost.
2. We provide comprehensive theoretical analysis to establish error bounds for the proposed method when solving linear PDEs and some special nonlinear PDEs.

*Submitted to the editors 1/27/2023.

Funding: This work was supported in part by National Science Foundation under grants DMS-1925263 and DMS-2152960, and ONR N00014-21-1-2891.

[†]Department of Mathematics and Statistics, Georgia State University, Atlanta, GA, USA (ngaby1@gsu.edu).

[‡]Department of Mathematics and Statistics, Georgia State University, Atlanta, GA, USA (xye@gsu.edu).

[§]School of Mathematics, Georgia Institute of Technology, Atlanta, GA, USA (hmzhou@gatech.edu).

3. We conduct a series of numerical experiments to demonstrate the effectiveness of the proposed method in solving a variety of linear and nonlinear PDEs.

The remainder of this paper is organized as follows. In Section 2, we provide an overview of recent neural network based numerical methods for solving PDEs. We outline the fundamentals of our proposed approach in Section 3.1 and provide details of our method and its key characteristics in Section 3.2. We conduct comprehensive error analysis in Section 3.3. We demonstrate the performance of the proposed method on several linear and nonlinear evolution PDEs in Section 4. Some variations and generalizations of the proposed approach are given in Section 5. Finally, Section 6 concludes this paper.

2. Related Work.

2.1. Classical methods for solving PDEs. Classical numerical methods for solving PDEs, such as finite difference [76] and finite element methods [40], discretize the spatial domain using mesh or triangulation. These methods convert a PDE to its discrete counterpart, which is a system of algebraic equations with finite number of unknowns, and solve the system to obtain approximate solution on the grid points [1, 22, 66, 75]. These methods have been significantly advanced in the past decades, and they are able to handle complicated situations such as irregular domains. However, they severely suffer “curse of dimensionality” when applied to high-dimensional problems—the number of unknowns increases exponentially fast with respect to spatial dimension, which renders them computationally intractable for many problems.

2.2. Neural network based methods for solving PDEs. Early attempts using neural networks to solve PDEs can be seen in [17, 43–45]. DNNs emerged in recent years and demonstrated striking power in solving PDEs through various approaches [5, 7, 21, 50, 61, 69, 70, 72, 78, 79, 82, 85, 86]. DNNs, which are the key machinery of deep learning, have demonstrated extraordinary potential in solving many high-dimensional nonlinear PDEs, which were considered computationally intractable using classical methods. For example, a variety of DNN based methods have been proposed based on strong form [7, 17, 41, 57, 59, 62, 63, 69, 70], variational form [21], and weak form [5, 85] of PDEs. They are considered with adaptive collocation strategy [3], adversarial inference procedure [83], oscillatory solutions [12], and multiscale methods [13, 52, 77]. Improvements of these methods with adaptive activation functions [39], networks structures [26, 27, 36], boundary conditions [18, 56], structure probing [36], as well as their convergence [55, 71], are also studied.

For a class of high-dimensional PDEs which have equivalent backward stochastic differential equation (SDE) formulations due to Feynman-Kac theory, deep learning methods have been applied by leveraging such correspondences [6, 20, 25, 30–32, 37, 38, 65]. These methods are shown to be good even in high dimensions [31, 37, 65], however, they can only solve for a solution $u(x)$ for a single x at a time.

For evolution PDEs, parameter evolution algorithms [2, 10, 19] have also been considered. These methods parameterize the PDE solution as neural network [10, 19] or an adaptively chosen ansatz as discussed in [2]. In these methods, the parameters are evolved forward in time through a time marching scheme, where at each step a linear system [10, 19] or a constrained optimization problem [2] needs to be solved.

2.3. Learning solution operator of PDEs. The aforementioned methods aim at solving specific instance of a given PDE, and they need to be rerun from scratch when any of the problem configuration (e.g., initial value, boundary value, problem domain) changes. In contrast, the solution operator of a PDE directly maps a problem configuration to its corresponding solution. To this end, several methods have been proposed to approximate Green’s functions for some linear PDEs [8, 9, 51, 74], as solutions to such PDEs have explicit expression based on their Green’s functions. However, this approach only applies to a small class of linear PDEs whose solution can be represented using Green’s functions. Moreover, Green’s functions have singularities and it requires special care to approximate them using neural networks. For example, rational functions are used as activation functions of DNNs to address singularities in [8]. In [9], the singularities are represented with the help of fundamental solutions.

For general nonlinear PDEs, DNNs have been used for operator approximation and meta-learning for PDEs [11, 14, 15, 24, 42, 47, 48, 53, 54, 58, 62, 80, 81]. For example, DeepONets [53] seek to approximate solution mappings by use of a “branch” and “trunk” network, while FNOs [47] use Fourier transforms to map a neural network to a low dimensional space and then back to the solution. Both methods require discretization of the infinite-dimensional function space, and they potentially require a large number of labeled data-solution pairs obtained through other methods or examples with explicitly known solutions.

2.4. Differences between our proposed approach and existing ones. Different from all existing approaches, we propose to approximate solution operators of evolution PDEs in a control framework in parameter spaces induced by general reduced-order models such as DNNs. Unlike the existing solution operator approximation methods (e.g., DeepONet [53] and FNO [47]) which seek to directly approximate the infinite-dimensional operator, our approach is based on the relation between evolving solutions and their projected trajectories in the parameter space. This leads us to transform the problem of finding a solution operator into a control vector field optimization problem. As a result, the problem of solving an evolution PDE in continuous space is reduced to numerically solving a system of ODEs, which can be done accurately with very low computation complexity. Moreover, our approach does not require any spatial discretization nor need any basis function representation and thus has great potential to solve evolution PDEs in high-dimensional cases. This is a significant advantage over existing operator learning methods such as DeepONet or FNOs as their spatial discretization schemes, which are used to generate the training data, hinder their application to high-dimensional cases.

3. Proposed Method. The main goal of this paper is to develop a new computational framework to approximate the *solution operator* for IVPs of high-dimensional evolution PDEs. The solution operator is a procedure that, once known, can efficiently map an arbitrarily given initial value g to the solution of the IVP without solving the PDE again. We first propose to parameterize u as a *nonlinear reduced-order model*, such as a DNN, which is denoted by u_θ with parameter θ , i.e., u_θ is a parametric function determined by the value of its finite-dimensional parameter θ , and u_θ is used to approximate u .

To find the solution operator, we propose to build a control vector field V in the parameter space Θ where θ resides. Then the solution operator can be implemented as a fast numerical solver of the ODE defined by V . More precisely, we first find the parameter θ_0 such that u_{θ_0} approximates g , then we follow the control vector field V to obtain a trajectory $\{\theta_t \mid 0 \leq t \leq T\}$ in Θ with very low computational cost, which automatically induces a trajectory u_{θ_t} to approximate the true solution u of the IVP with the initial value g . We provide details of these constructions in the following subsections.

3.1. Nonlinear reduced-order models and parameter submanifold. Reduced-order models, such as DNNs, have emerged as a powerful tool to solve high-dimensional PDEs in recent years [5, 21, 30, 67–69, 85]. Mathematically, a DNN can be expressed as the composition of a series of simple linear and nonlinear functions. In the deep learning context, a typical building block of DNNs is called a layer, which is a mapping $h : \mathbb{R}^d \rightarrow \mathbb{R}^{d'}$ for some compatible input dimension d and output dimension d' :

$$(3.1) \quad h(z; W, b) := \sigma(Wz + b),$$

where $z \in \mathbb{R}^d$ is the input variable of h , the matrix $W \in \mathbb{R}^{d' \times d}$ and vector $b \in \mathbb{R}^{d'}$ are called the weight and bias respectively, and $\sigma : \mathbb{R} \rightarrow \mathbb{R}$ is a nonlinear function that operates componentwise on its d' -dimensional argument vector $Wz + b$ (hence σ is effectively a mapping from $\mathbb{R}^{d'}$ to $\mathbb{R}^{d'}$). Common choices of activation functions include the sigmoid $\sigma(z) = (1 + e^{-z})^{-1}$, hyperbolic tangent (tanh) $\sigma(z) = (e^z - e^{-z})/(e^z + e^{-z})$, rectified linear unit (ReLU) $\sigma(z) = \max(0, z)$, rectified power unit (RePU) $\sigma(z) = \max(0, z)^p$ for $p > 0$, swish function $\sigma(z) = z(1 + e^{-z})^{-1}$, rational functions, and many others. We only consider smooth activation functions σ hereafter. A commonly used DNN structure u_θ , often called feed-forward network (FFN), is defined as the composition of multiple layer functions of form (3.1) as follows:

$$(3.2) \quad u_\theta(x) := u(x; \theta) = w^\top z_L + b, \\ \text{where } z_0 = x, \quad z_l = h_l(z_{l-1}) := h(z_{l-1}; W_l, b_l), \quad l = 1, \dots, L,$$

and the l th hidden layer $h(\cdot; W_l, b_l) : \mathbb{R}^{d_{l-1}} \rightarrow \mathbb{R}^{d_l}$ is determined by its weight and bias parameters $W_l \in \mathbb{R}^{d_l \times d_{l-1}}$ and $b_l \in \mathbb{R}^{d_l}$ for $l = 1, \dots, L$ and $d_0 = d$. Here the output of u_θ is set to the affine transform of the last hidden layer $z_{NN} = h_L(z_{L-1})$ using weight $w \in \mathbb{R}^{d_L}$ and bias $b \in \mathbb{R}$. The *network parameter* θ refers to the collection of all learnable parameters (stacked as a vector in \mathbb{R}^m) of u_θ , i.e.,

$$(3.3) \quad \theta := (w, b, W_L, b_L, \dots, W_1, b_1) \in \mathbb{R}^m,$$

and training the network u_θ refers to finding the minimizer θ of some properly designed loss function.

DNNs are shown to be very powerful in approximating high-dimensional functions in a vast amount of studies in recent years, see, e.g., [28, 29, 34, 35, 46, 49, 64, 84]. For example, it is shown in [28] that for any

$M, \varepsilon > 0$, $k \in \mathbb{N}$, $p \in [1, \infty]$, and $\Omega = (0, 1)^d \subset \mathbb{R}^d$, denote $F := \{f \in W^{k,p}(\Omega; \mathbb{R}) \mid \|f\|_{W^{k,p}(\Omega)} \leq M\}$, then there exists a DNN structure u_θ of form (3.2) with sufficiently large m and L (which depend on M, ε, d and p only), such that for any $f \in F$, there is $\|u_\theta - f\|_{W^{k,p}(\Omega)} \leq \varepsilon$ for some $\theta \in \mathbb{R}^m$. This result implies that $\{u_\theta \mid \theta \in \mathbb{R}^m\}$ is an ε -net of the M -ball of the Sobolev space $W^{k,p}(\Omega)$, suggesting that DNNs are suitable to approximate solutions of PDEs. This is one of the many error bounds established in recent years, and such bounds are still being continuously improved nowadays.

Our approach relies on the key relation between the parameter θ and the reduced-order model u_θ . More specifically, we identify the finite-dimensional parameter space $\Theta \subset \mathbb{R}^m$ where θ belongs to and the submanifold \mathcal{M} of functions defined by

$$(3.4) \quad \mathcal{M} := \{u_\theta : \Omega \rightarrow \mathbb{R} \mid \theta \in \Theta\}.$$

As we can see, u_θ defines a mapping from the parameter space Θ to the submanifold \mathcal{M} of the infinite-dimensional function space. We call \mathcal{M} the *parameter submanifold* determined by u_θ .

To approximate a time-evolving function $u^*(\cdot, t)$, e.g., the solution of an evolution PDE, over time horizon $[0, T]$ using the reduced-order model u_θ , we need to find a trajectory $\{\theta_t \in \Theta \mid 0 \leq t \leq T\}$ in the parameter space Θ so that $u_{\theta_t}(\cdot)$ is close to $u^*(\cdot, t)$ in the function space for every $t \in [0, T]$. For example, if we consider $L^2(\Omega)$ as the function space, by closeness we mean $\|u_{\theta_t} - u^*(\cdot, t)\|_{L^2(\Omega)}$ is small for all t (hereafter we denote $\|\cdot\|_p = \|\cdot\|_{L^p(\Omega)}$ for notation simplicity). Notice that $\{u_{\theta_t} \mid 0 \leq t \leq T\}$ is a trajectory on \mathcal{M} , whereas $u^*(\cdot, t)$ is a trajectory in the full space $L^2(\Omega)$.

3.2. Proposed methodology. Let $\Omega = (0, 1)^d$ be the unit open cube in \mathbb{R}^d and F a *nonlinear differential operator* of functions $u : \Omega \rightarrow \mathbb{R}$ with necessary regularity conditions, we consider the IVP of the evolution PDE defined by F with arbitrary initial value as follows:

$$(3.5) \quad \begin{cases} \partial_t u(x, t) = F[u](x, t), & x \in \Omega, t \in (0, T], \\ u(x, 0) = g(x), & x \in \Omega, \end{cases}$$

where $T > 0$ is some prescribed terminal time, and $g : \mathbb{R}^d \rightarrow \mathbb{R}$ stands for an initial value. For ease of presentation, we assume zero Dirichlet boundary condition $u(x, t) = 0$ for all $x \in \bar{\Omega}$ and $t \in [0, T]$ (for compatibility we henceforth assume $g(x)$ has zero trace on $\partial\Omega$) throughout this paper. We denote u^g the solution to the IVP (3.5) with this initial g . The solution operator \mathcal{S}_F of the IVP (3.5) is thus the mapping from the initial g to the solution u^g :

$$(3.6) \quad \mathcal{S}_F : C^2(\bar{\Omega}) \rightarrow C^{2,1}(\bar{\Omega} \times [0, T]), \quad \text{such that } g \mapsto \mathcal{S}_F(g) := u^g,$$

where $C^2(\bar{\Omega}) := C(\bar{\Omega}) \cap C^2(\Omega)$ for short. Our goal is to find a numerical approximation to \mathcal{S}_F . Namely, we want to find a fast computational scheme \mathcal{S}_F that takes any initial g as input and accurately estimate u^g with low computation complexity.

It is important to note the substantial difference between solving (3.5) for any given but fixed initial value g and finding the solution operator (3.6) that maps any g to the corresponding solution u^g . In the literature, most methods are developed for solving IVP (3.5) with a fixed g , such as traditional finite difference and finite element methods, as well as many state-of-the-art machine learning based methods. However, these methods are computationally expensive if (3.5) must be solved with many different initial values, and they need to start from scratch for every new g . In a sharp contrast, our goal is to find an approximation to the solution operator \mathcal{S}_F which, once found, can help us to compute u^g for any given g at relatively much lower computational cost.

For ease of presentation, we use autonomous, second-order nonlinear differential operators $F[u] = F(x, u, \nabla_x u, \nabla_x^2 u)$ as an example and take $\Omega = (0, 1)^d$ in (3.5) to describe our main idea below. Extensions to general non-autonomous nonlinear differential operators and PDEs defined on open bounded set $\Omega \subset \mathbb{R}^d$ with given boundary values will be discussed in Section 5.

To approximate the solution operator \mathcal{S}_F in (3.6), we propose a *control mechanism in the parameter space* Θ of a prescribed reduced-order model u_θ . Specifically, we first determine a reduced-order model u_θ to represent solutions of the IVP. We allow any parametric form of u_θ but only assume that $u_\theta(x) = u(x; \theta)$ is

C^1 smooth with respect to θ . This is a mild condition satisfied by the commonly used reduced-order models: if u_θ is a linear combination of basis functions and θ represents the combination coefficients, then u_θ is linear and hence smooth in θ ; and if u_θ is a DNN as in (3.2), then u_θ is smooth in θ as long as all activation functions σ are smooth. Suppose there exists a trajectory $\{\theta_t | 0 \leq t \leq T\}$ in the parameter space Θ such that its corresponding u_{θ_t} approximates the solution of the IVP, we must have

$$(3.7) \quad \begin{cases} \partial_t u_{\theta_t}(x) = \nabla_\theta u(x; \theta_t) \cdot \dot{\theta}_t = F[u_{\theta_t}](x), & \forall x \in \Omega, t \in (0, T], \\ u_{\theta_0}(x) = g(x), & \forall x \in \Omega. \end{cases}$$

To compute u_{θ_t} , it is sufficient to find a control vector (velocity) field $V_F : \Theta \rightarrow \mathbb{R}^m$, in the sense of $\dot{\theta}_t = V_F(\theta_t)$, that steers the trajectory θ_t along the correct direction starting from the initial θ_0 satisfying $u_{\theta_0}(x) = g(x)$.

This observation suggests a new approach to solve the IVP with a fixed evolution PDE but varying initial values g : for the evolution equation in (3.7) to hold, it suffices to find a vector field V_F such that

$$(3.8) \quad \nabla_\theta u_\theta \cdot V_F(\theta) = F[u_\theta]$$

for all $\theta \in \Theta$. It is important to note that V_F only depends on the nonlinear differential operator F of the original evolution PDE, but not any actual initial value g of the IVP. Once this is achieved, we can effectively approximate the solution of the IVP with any initial value g : we first set $\theta_0 = \theta^g$, where θ^g denotes the parameter such that u_{θ^g} fits g , then we numerically solve the following ODE in the parameter space Θ (which can be fast) using the control vector field V_F :

$$(3.9) \quad \begin{cases} \dot{\theta}_t = V_F(\theta_t), & \forall t \in (0, T], \\ \theta_0 = \theta^g. \end{cases}$$

The solution trajectory $\{\theta_t | 0 \leq t \leq T\}$ of the ODE (3.9) induces a path $\{u_{\theta_t} | 0 \leq t \leq T\}$ in \mathcal{M} as an approximation to the solution of the IVP. The computational cost is thus composed of two parts: finding the parameter θ^g of u_θ to fit g and numerically solving the ODE (3.9), both of which are substantially cheaper than solving the IVP (3.5).

The main question is how to get the control vector field V_F in (3.9). As an explicit form of V_F is unknown, we choose to express V_F in a general parametric form V_ξ with parameter ξ to be determined. Specifically, we propose to set V_ξ as another DNN where ξ represents the set of learnable network parameters in V_ξ . We call V_ξ the *neural control* field. We learn the parameter ξ by minimizing the following loss function:

$$(3.10) \quad \ell(\xi) := \int_\Theta \|\nabla_\theta u_\theta \cdot V_\xi(\theta) - F[u_\theta]\|_2^2 d\theta.$$

In practice, we approximate the integral in ℓ by Monte Carlo integration. We sample K points $\{\theta_k | k = 1, \dots, K\}$ uniformly from Θ (here the subscript k in θ_k stands for the k th point among the K points sampled in Θ) and form the empirical loss function

$$(3.11) \quad \hat{\ell}(\xi) = K^{-1} \cdot \sum_{k=1}^K \|\nabla_\theta u_{\theta_k} \cdot V_\xi(\theta_k) - F[u_{\theta_k}]\|_2^2$$

Then we minimize $\hat{\ell}(\xi)$ with respect to ξ , where the L^2 norm is also approximated by Monte Carlo integration on Ω . The training of V_ξ is summarized in Algorithm 3.1.

Once we trained the vector field V_ξ , we can implement the solution operator \mathcal{S}_F in the following two steps: we first find a θ_0 such that u_{θ_0} fits g , i.e., find θ_0 that minimizes $\|u_{\theta_0} - g\|_2$. This can be done by sampling $\{x_n\}_{n=1}^N$ from Ω and minimizing the empirical squared L^2 norm $(1/N) \cdot \sum_{n=1}^N |u_{\theta_0}(x_n) - g(x_n)|^2$ with respect to θ . Then we solve the ODE (3.9) using any numerical ODE solver (e.g., Euler, 4th order Runge-Kutta, predictor-corrector) with θ_0 as the initial value. Both steps can be done efficiently and the total computational cost is substantially lower than that of solving the original IVP (3.5) again. We summarize how neural control solves IVPs in Algorithm 3.2.

Algorithm 3.1 Training neural control V_ξ

Input: Reduced-order model structure u_θ and parameter set Θ . Control vector field structure V_ξ . Error tolerance ε .

Output: Optimal control parameter ξ .

- 1: Sample $\{\theta_k\}_{k=1}^K$ uniformly from Θ and $\{x_n\}_{n=1}^N$ from Ω .
- 2: Form empirical loss $\hat{\ell}(\xi)$ as in (4.2).
- 3: Minimize $\hat{\ell}$ with respect to ξ using any optimizer (e.g., ADAM or AdaGrad) until $\hat{\ell}(\xi) \leq \varepsilon$.

Algorithm 3.2 Implementation of solution operator \mathcal{S}_F of the IVP (3.5) using trained control V_ξ

Input: Initial value g and tolerance ε_0 . Reduced-order model u_θ and trained neural control V_ξ .

Output: Trajectory $\hat{\theta}_t$ such that $u_{\hat{\theta}_t}$ approximate the solution $\mathcal{S}_F[g]$ of the IVP (3.5).

- 1: Compute initial parameter θ_0 such that $\|u_{\theta_0} - g\|_2 \leq \varepsilon_0$.
- 2: Use any ODE solver to compute $\hat{\theta}_t$ to solve (3.9) with approximate field V_ξ and initial θ_0 .

3.3. Error analysis. In this subsection, we develop an error estimate of the proposed method. We first focus on the error due to projection onto the tangent space $T_{u_\theta}\mathcal{M}$ in the L^2 space in Section 3.3.1. Then we establish the solution approximation error for linear and semilinear parabolic PDEs in Section 3.3.2. For ease of discussion, we again assume zero Dirichlet boundary condition $u(x, t) = 0$ for all $x \in \bar{\Omega}$ and $t \in [0, T]$, and we let $\Omega = (0, 1)^d \subset \mathbb{R}^d$ be the unit open cube in \mathbb{R}^d and Θ some open bounded set in \mathbb{R}^m . We let $F[u] := F(u, \nabla u, \nabla^2 u)$ be a nonlinear differential operator with necessary regularity conditions to be specified later. Additional requirements on the regularity of u_θ will be given when needed.

3.3.1. Approximation error of control vector field. We first investigate the main source of error when using a reduced-order model to approximate the time-evolving solution of the given PDE. We show that this error is due to the imperfect representation of $F[u_\theta]$ using $\nabla_\theta u_\theta$ in (3.8). Specifically, due to the approximation of reduced-order models, $T_{u_\theta}\mathcal{M}$ is only a finite-dimensional subspace of L^2 , and thus we can only approximate the projection of $F[u_\theta]$ onto this tangent space. We will need the following assumptions on the regularity of u_θ and F .

ASSUMPTION 1. *The reduced-order model $u_\theta(\cdot) \in C^3(\Omega) \cap C(\bar{\Omega})$ for every $\theta \in \bar{\Theta}$ and $u(x; \cdot) \in C^1(\Theta) \cap C(\bar{\Theta})$. Moreover, there exists $L > 0$ such that for all $\theta \in \bar{\Theta}$*

$$(3.12) \quad F[u_\theta] \in \mathcal{F}^L := \{f \in C^1(\Omega) \cap C(\bar{\Omega}) : \|f\|_\infty \leq L, \|\nabla f\|_\infty \leq L\}.$$

Assumption 1 provides some sufficient regularity conditions on the reduced-order model u_θ and boundedness of $F[u_\theta]$ and its gradient to be used in our error estimates. Notice that we consider F as second-order differential operator here and therefore the assumption $u_\theta \in C^3(\Omega)$ ensures that $u_\theta(x), \nabla u_\theta(x), \nabla^2 u_\theta(x)$ are all sufficiently smooth. The regularity condition on F in Assumption 1 requires that the mapping $F[u_\theta](x)$ is a C^1 function and have magnitudes and gradients bounded by L over $\bar{\Omega}$. These assumptions are generally mild as we will use reduced-order models smooth in (x, θ) , e.g., a DNN with smooth activation functions, and the operator F is sufficiently regular.

ASSUMPTION 2. *For any $\bar{\varepsilon} > 0$, there exist a reduced-order model u_θ and a bounded open set $\Theta \subset \mathbb{R}^m$, such that for every $\theta \in \bar{\Theta}$ there exists a vector $v_\theta \in \mathbb{R}^m$ satisfying*

$$\|v_\theta \cdot \nabla_\theta u_\theta - F[u_\theta]\|_2 \leq \bar{\varepsilon}.$$

Assumption 2 provides an upper bound on the error when projecting $F[u_\theta]$ onto the tangent space $T_{u_\theta}\mathcal{M}$, which is spanned by the functions in $\nabla_\theta u_\theta$. This error bound is determined by the choice of the reduced-order model u_θ and the parameter set Θ . As will be demonstrated in our numerical experiments, a small projection error can be achieved by using standard DNN as reduced-order model u_θ . As such error is difficult to analyze due to the complex structures of general DNNs. We provide an example reduced-order model with special structure to justify the reasonableness of Assumption 2.

EXAMPLE 3.1. Let $\bar{\varepsilon} > 0$ and $\{\varphi_j\}_{j=1}^{\infty}$ be a complete smooth orthonormal basis (e.g., generalized Fourier basis) for $L^2(\Omega)$. Suppose there exist $C > 0$, $\gamma > 1$, and $C_0 > 0$ such that for all $u \in C^3(\Omega) \cap C(\bar{\Omega})$ and $\|u\|_2^2 \leq C_0$ we have

$$(3.13) \quad F[u] \in \mathcal{G}^{C,\gamma} := \left\{ f \in C^1(\Omega) \cap C(\bar{\Omega}) : |\langle f, \varphi_j \rangle|^2 \leq Cj^{-\gamma}, \forall j \geq 1 \right\}.$$

Consider $u_\theta = \theta \cdot \varphi = \sum_{j=1}^m \theta_j \varphi_j$. We denote $f_\theta := F[u_\theta]$ for short. Then there exists $m = m(\bar{\varepsilon}, C, \gamma) \in \mathbb{N}$ such that $\sum_{j=m+1}^{\infty} Cj^{-\gamma} < \bar{\varepsilon}^2$. Then $\nabla_\theta u_\theta = \varphi = (\varphi_1, \dots, \varphi_m)$ and for $\alpha^{f_\theta} = (\alpha_1^{f_\theta}, \dots, \alpha_m^{f_\theta})$ with $\alpha_j^{f_\theta} := \langle f_\theta, \varphi_j \rangle$, there is

$$\|\alpha^{f_\theta} \cdot \nabla_\theta u_\theta - F[u_\theta]\|_2^2 = \left\| \sum_{j=1}^m \alpha_j^{f_\theta} \varphi_j - f_\theta \right\|_2^2 = \sum_{j=m+1}^{\infty} |\langle f_\theta, \varphi_j \rangle|^2 \leq \bar{\varepsilon}^2.$$

Therefore, the reduced-order model $u_\theta = \theta \cdot \varphi$ with $\Theta = \{\alpha \in \mathbb{R}^m : |\alpha|^2 < C_0\}$ and $v_\theta = \alpha^{f_\theta}$ satisfy Assumption 2.

This example can be modified to use a more general form of reduced-order model u_θ , such as a DNN. To see this, we first repeat the procedure above but with $\bar{\varepsilon}$ replaced by $\bar{\varepsilon}/2$. Then the universal approximation theorem [34, 84] and the continuity of DNNs in its parameters imply that there exist DNNs $\{\hat{\varphi}_j : 1 \leq j \leq m\}$, whose network parameters are collectively denoted by $\eta \in \mathbb{R}^{m'}$, satisfy $\|\hat{\varphi}_j - \varphi_j\|_\infty \leq \bar{\varepsilon}/(2\sqrt{mC_0}|\Omega|)$ and hence $\|\hat{\varphi}_j - \varphi_j\|_2 \leq \bar{\varepsilon}/(2\sqrt{mC_0})$ for all η in an open set $H \subset \mathbb{R}^{m'}$. Consider the DNN $u_\theta = c \cdot \hat{\varphi}$ with parameter $\theta = (c, \eta) \in \mathbb{R}^n$ where $n = m + m'$. Then $\nabla_c u_\theta(x) = (\hat{\varphi}_1, \dots, \hat{\varphi}_m)$. Using the example above, we know for any $f_\theta := F[u_\theta] \in \mathcal{G}^{C,\gamma}$, there exists $\alpha^{f_\theta} \in \mathbb{R}^m$ such that $\|\alpha^{f_\theta} \cdot \varphi - F[u_\theta]\|_2 \leq \bar{\varepsilon}/2$. Therefore, we use $(\alpha^{f_\theta}, 0)$ which concatenates α^{f_θ} and $0 \in \mathbb{R}^{m'}$ as the combination coefficients of $\nabla_\theta u_\theta$ to obtain

$$\begin{aligned} \|(\alpha^{f_\theta}, 0) \cdot \nabla_\theta u_\theta - F[u_\theta]\|_2 &= \|\alpha^{f_\theta} \cdot \nabla_c u_\theta - F[u_\theta]\|_2 \\ &\leq \|\alpha^{f_\theta} \cdot \hat{\varphi} - \alpha^{f_\theta} \cdot \varphi\|_2 + \|\alpha^{f_\theta} \cdot \varphi - F[u_\theta]\|_\infty \\ &\leq \sum_{j=1}^m |\alpha_j^{f_\theta}| \|\hat{\varphi}_j - \varphi_j\|_2 + \frac{\bar{\varepsilon}}{2} \\ &\leq \sqrt{mC_0} \cdot \frac{\bar{\varepsilon}}{2\sqrt{mC_0}} + \frac{\bar{\varepsilon}}{2} \\ &= \bar{\varepsilon}. \end{aligned}$$

Therefore, the DNN $u_\theta = c \cdot \hat{\varphi}$ with $\Theta = \{(c, \eta) : |c_j|^2 < C_0, \eta \in H\}$ and $v_\theta = (\alpha^{f_\theta}, 0)$ satisfy Assumption 2.

Before proving the main proposition of this section we will need the following lemma.

LEMMA 3.2. Suppose Assumption 1 and 2 are satisfied. For all $\varepsilon > \bar{\varepsilon}$ there exists $v : \bar{\Theta} \rightarrow \mathbb{R}^m$ such that v is bounded over $\bar{\Theta}$ and

$$\|v_\theta \cdot \nabla_\theta u_\theta - F[u_\theta]\|_2 \leq \varepsilon.$$

Proof. Let $\varepsilon > \bar{\varepsilon}$ and $\delta \in (0, \varepsilon - \bar{\varepsilon})$. By Assumption 2, for all $\theta \in \Theta$ there exists $\alpha_\theta \in \mathbb{R}^m$ coefficient such that

$$\|\alpha_\theta \nabla_\theta u_\theta - F[u_\theta]\|_2 \leq \bar{\varepsilon}.$$

As $F[u_\theta]$ and $\nabla_\theta u_\theta$ are continuous and Ω is bounded, we associate to each θ and coefficient α_θ the open set U_θ containing θ , small enough, such that for all $\theta' \in U_\theta$ we have

$$(3.14) \quad \|\alpha_\theta \nabla_\theta u_{\theta'} - \alpha_\theta \nabla_\theta u_\theta\|_2 + \|F[u_\theta] - F[u_{\theta'}]\|_2 \leq \delta$$

and hence

$$(3.15) \quad \|\alpha_\theta \cdot \nabla_\theta u_{\theta'} - F[u_{\theta'}]\|_2 \leq \|\alpha_\theta \nabla_\theta u_{\theta'} - \alpha_\theta \nabla_\theta u_\theta\|_2 + \|\alpha_\theta \nabla_\theta u_\theta - F[u_\theta]\|_2 + \|F[u_\theta] - F[u_{\theta'}]\|_2 \leq \delta + \bar{\varepsilon}.$$

Therefore $\cup_{\theta \in \bar{\Theta}} U_\theta$ is an open cover of $\bar{\Theta}$. As $\bar{\Theta}$ is compact this open cover has a finite subcover $\cup_{i=1}^N U_{\theta_i}$ for particular θ_i 's. Define $v : \bar{\Theta} \rightarrow \mathbb{R}^m$ such that $v_\theta = \alpha_{\theta_i}$ if $\theta \in U_{\theta_i}$ (if θ is in the intersection of multiple U_{θ_i} 's we choose a single α_{θ_i} arbitrarily). We see from this construction that v_θ is bounded over $\bar{\Theta}$ as the range of v_θ is finite. From (3.15) we have

$$\|v_\theta \cdot \nabla_\theta u_\theta - F[u_\theta]\|_2 \leq \delta + \bar{\varepsilon} \leq \varepsilon. \quad \square$$

With Assumptions 1 and 2, and Lemma 3.2 we can prove the existence of an accurate neural control field V_ξ parameterized as a neural network, as shown in the next proposition.

PROPOSITION 3.3. *Suppose Assumption 1 and 2 hold. Then for any $\varepsilon > 0$, there exists a differentiable vector field parameterized as a neural network $V_\xi : \bar{\Theta} \rightarrow \mathbb{R}^m$ with parameter ξ , such that*

$$\|V_\xi(\theta) \cdot \nabla_\theta u_\theta - F[u_\theta]\|_2 \leq \varepsilon,$$

for all $\theta \in \bar{\Theta}$.

Proof. We first show that there exists a differentiable vector-valued function $V : \bar{\Theta} \rightarrow \mathbb{R}^d$ such that

$$(3.16) \quad \|V(\theta) \cdot \nabla_\theta u_\theta - F[u_\theta]\|_2 \leq \frac{\varepsilon}{2}$$

for all $\theta \in \bar{\Theta}$. To this end, we choose $\bar{\varepsilon}_0 \in (0, \varepsilon/2)$ and $\bar{\varepsilon} \in (\bar{\varepsilon}_0, \varepsilon/2)$, then by Assumption 2 and Lemma 3.2 we know that there exist a reduced-order model u_θ , a bounded open set $\Theta \subset \mathbb{R}^m$, and $M_v > 0$ such that there is a vector-valued function $\theta \mapsto v_\theta$, where for any $\theta \in \bar{\Theta}$, we have $|v_\theta| < M_v$ and

$$\|v_\theta \cdot \nabla_\theta u_\theta - F[u_\theta]\|_2 \leq \bar{\varepsilon}.$$

Note that v_θ is not necessarily differentiable with respect to θ . To obtain a differentiable vector field $V(\theta)$, for each $\theta \in \bar{\Theta}$, we define the function ψ_θ by

$$\psi_\theta(w) := \|w \cdot \nabla_\theta u_\theta - F[u_\theta]\|_2^2 = w^\top G(\theta)w - 2w^\top p(\theta) + q(\theta),$$

where

$$(3.17) \quad G(\theta) := \int_{\Omega} \nabla_\theta u_\theta(x) \nabla_\theta u_\theta(x)^\top dx, \quad p(\theta) := \int_{\Omega} \nabla_\theta u_\theta(x) F[u_\theta](x) dx, \quad q(\theta) := \int_{\Omega} F[u_\theta](x)^2 dx.$$

Then we know

$$(3.18) \quad \psi_\theta^* := \psi_\theta(v_\theta) = \|v_\theta \cdot \nabla_\theta u_\theta - F[u_\theta]\|_2^2 \leq \bar{\varepsilon}^2.$$

It is also clear that $G(\theta)$ is symmetric and positive semi-definite. Moreover, due to the compactness of $\bar{\Omega}$ and $\bar{\Theta}$, as well as that $\nabla_\theta u \in C(\bar{\Omega} \times \bar{\Theta})$, we know there exists $\lambda_G > 0$ such that

$$\|G(\theta)\|_2 \leq \lambda_G$$

for all $\theta \in \bar{\Theta}$. Therefore, ψ_θ is a convex function and the Lipschitz constant of $\nabla \psi_\theta$ is uniformly upper bounded by λ_G over $\bar{\Theta}$. Now for any $w \in \mathbb{R}^m$, $h > 0$, and $K \in \mathbb{N}$ (we reuse the letter K as the iteration counter instead of the number of sampling points in this proof), we define

$$\mathcal{O}_\theta^{K,h}(w) := w_K, \quad \text{where} \quad w_k = w_{k-1} - h \nabla \psi_\theta(w_{k-1}), \quad w_0 = w, \quad k = 1, \dots, K.$$

Namely, $\mathcal{O}_\theta^{K,h}$ is the oracle of executing the gradient descent optimization scheme on ψ_θ with step size $h > 0$ for K iterations.

Hence, adopting the standard convergence result of gradient descent in convex optimization [60, Theorem 2.1.14] using ψ_θ^* and combined with the bound $|v_\theta| < M_v$ we obtain for any fixed $h \in (0, 1/\lambda_G)$ and

$$K \geq \frac{2M_v^2}{h(2 - \lambda_G h)((\varepsilon/2)^2 - \bar{\varepsilon}^2)},$$

there is

$$(3.19) \quad \psi_\theta(\mathcal{O}_\theta^{K,h}(0)) - \psi_\theta^* \leq \frac{2M_v^2}{Kh(2 - \lambda_G h)} \leq \left(\frac{\varepsilon}{2}\right)^2 - \bar{\varepsilon}^2.$$

Notice that $\mathcal{O}_\theta^{K,h}$ is a differentiable vector-valued function of θ because K and h are fixed. Therefore, combining (3.18) and (3.19) yields

$$0 \leq \psi_\theta(\mathcal{O}_\theta^{K,h}(0)) = (\psi_\theta(\mathcal{O}_\theta^{K,h}(0)) - \psi_\theta^*) + \psi_\theta^* \leq (\varepsilon/2)^2 - \bar{\varepsilon}^2 + \bar{\varepsilon}^2 = (\varepsilon/2)^2.$$

As this inequality holds $\theta \in \bar{\Theta}$, we set $V(\theta) = \mathcal{O}_\theta^{K,h}(0)$ which is a differentiable function of θ satisfying (3.16).

By the universal approximation theorem of neural networks [34], we know there exists a differentiable vector-valued function parameterized as a neural network V_ξ with parameter ξ such that

$$|V_\xi(\theta) - V(\theta)|_\infty \leq \varepsilon/(2B)$$

for all $\theta \in \bar{\Theta}$, where $B := \max_{\theta \in \bar{\Theta}} \|\nabla_\theta u_\theta\|_2 < \infty$ and $|\cdot|_\infty$ stands for the ∞ -norm of vectors. Hence we know

$$\|V_\xi(\theta) \cdot \nabla_\theta u_\theta - F[u_\theta]\|_2 \leq \|V_\xi(\theta) \cdot \nabla_\theta u_\theta - V(\theta) \cdot \nabla_\theta u_\theta\|_2 + \|V(\theta) \cdot \nabla_\theta u_\theta - F[u_\theta]\|_2 \leq B \cdot \frac{\varepsilon}{2B} + \frac{\varepsilon}{2} = \varepsilon.$$

This completes the proof. \square

Remark 3.4. It is important to note the geometry of \mathcal{M} , especially its dimensionality, is complex and highly dependent on the structure of u_θ and the parameter space Θ . In particular, we can show that the tangent space $T_{u_\theta}\mathcal{M} = \text{span}(\nabla_\theta u_\theta)$ at any $u_\theta \in \mathcal{M}$ is in the L^2 space, where $\nabla_\theta u_\theta = (\partial_{\theta_1} u_\theta, \dots, \partial_{\theta_m} u_\theta)$ for $\theta = (\theta_1, \dots, \theta_m)$. (Here we use discrete indices $1, \dots, m$ as subscripts of θ to indicate its components for notation simplicity. This is to be distinguished from the subscript t in θ_t which stands for time of the trajectory θ_t .) However, $\dim(T_{u_\theta}\mathcal{M})$ may vary across different u_θ on \mathcal{M} . For example, consider the reduced-order model u_θ parameterized as a DNN as in (3.2): when $w = 0$, we have $\theta = (0, b, \dots)$ and hence $\partial_{w_i} u_\theta = 0$ and $\partial_{b_l} u_\theta = 0$ for all $l = 1, \dots, L$. In this case, the m components of $\nabla_\theta u_\theta$ are *not* linearly independent, and $\dim(T_{u_\theta}\mathcal{M}) < m$ for such θ 's. This distinguishes our parameter submanifold from existing ones, such as [2], which assumes that the tangent space is always of full dimension m at any point of the submanifold. In our case, however, challenges and complications in dealing with the parameter submanifold \mathcal{M} can be avoided if we made such assumption, but it will lead to incorrect analysis and error estimation, which poses a major technical challenge for the proposed framework. Specifically, we note that the rank of $G(\theta)$ varies across Θ , and therefore the pseudoinverse $G(\theta)^+$ may be discontinuous. A major theoretical merit of Proposition 3.3 is that we can still ensure the existence of a differentiable control vector field in such case.

3.3.2. Error analysis in solving (semi-)linear parabolic PDEs. Now we are ready to provide error bounds of our method in solving a large class of linear and semilinear parabolic PDEs. This class of PDEs covers many types of reaction-diffusion equations, such as heat equations, Fisher's equation or the Allen-Cahn equation. The differential operator F in linear and semilinear parabolic PDEs has the form

$$F[u] = \nabla \cdot (A \nabla u) + b \cdot \nabla u + f(u)$$

where $A : \Omega \rightarrow \mathbb{R}^{d \times d}$ and $b : \Omega \rightarrow \mathbb{R}^d$ are continuous, $f : \mathbb{R} \rightarrow \mathbb{R}$ is L_f -Lipschitz and acts on $u(x)$ for each x . Moreover we assume that there exists $\lambda \geq 0$ and $B \geq 0$ such that

$$(3.20) \quad z^\top A(x) z \geq \lambda |z|^2, \quad \forall z \in \mathbb{R}^d, x \in \Omega,$$

and

$$(3.21) \quad \|\nabla \cdot b\|_\infty \leq B.$$

Furthermore, due to the smoothness of V_ξ and compactness of $\bar{\Theta}$, we know there exist $M_V > 0$ and $L_V > 0$ such that

$$(3.22) \quad \max_{\theta \in \bar{\Theta}} |V_\xi(\theta)| \leq M_V \quad \text{and} \quad \max_{\theta \in \bar{\Theta}} |\nabla_\theta V_\xi(\theta)| \leq L_V.$$

THEOREM 3.5. *Suppose Assumptions 1 and 2 hold. Then there exists control field V_ξ such that for any u^* satisfying the evolution PDE in (3.5) there is*

$$(3.23) \quad \|u_{\theta_t}(\cdot) - u^*(\cdot, t)\|_2 \leq e^{(L_f + B/2 - \lambda/C_p)t}(\varepsilon_0 + \varepsilon t)$$

for all t as long as $\theta_t \in \bar{\Theta}$, where θ_t is solved from the ODE (3.9) with V_ξ and initial θ_0 satisfying $\|u_{\theta_0}(\cdot) - u^*(\cdot, 0)\|_2 \leq \varepsilon_0$. Here C_p is a constant depending only on Ω .

Proof. We denote the residual

$$r(x, t) := \nabla_\theta u_{\theta_t}(x) \cdot V_\xi(\theta_t) - F[u_{\theta_t}](x).$$

Then by Proposition 3.3 we have $\|r(\cdot, t)\|_2 \leq \varepsilon$ for all t . Furthermore, we denote

$$\delta(x, t) := u_{\theta_t}(x) - u^*(x, t)$$

for all $(x, t) \in \bar{\Omega} \times [0, T]$ and $D(t) := \|\delta(\cdot, t)\|_2$, then there is

$$(3.24) \quad D'(t) = \left\langle \frac{\delta(\cdot, t)}{\|\delta(\cdot, t)\|_2}, \partial_t \delta(\cdot, t) \right\rangle.$$

Here we use the convention that $\delta(\cdot, t)/\|\delta(\cdot, t)\|_2 = 0$ if $\delta(\cdot, t) = 0$ a.e. By the definition of δ , we have

$$\begin{aligned} \partial_t \delta(x, t) &= \partial_t u_{\theta_t}(x) - \partial_t u^*(x, t) \\ &= \nabla_\theta u_{\theta_t}(x) \cdot \dot{\theta}_t - F[u^*](x, t) \\ &= \nabla_\theta u_{\theta_t}(x) \cdot V_\xi(\theta_t) - F[u^*](x, t) \\ &= F[u_{\theta_t}](x) - F[u^*](x, t) + r(x, t) \\ &= \nabla \cdot (A(x) \nabla \delta(x, t)) + b(x) \cdot \nabla \delta(x, t) + f(u_{\theta_t}(x)) - f(u^*(x, t)) + r(x, t). \end{aligned}$$

Therefore, we have

$$\begin{aligned} \langle \delta(\cdot, t), \partial_t \delta(\cdot, t) \rangle &= \int_\Omega \delta(x, t) (\nabla \cdot (A(x) \nabla \delta(x, t)) + b(x) \cdot \nabla \delta(x, t)) dx \\ &\quad + \int_\Omega \delta(x, t) (f(u_{\theta_t}(x)) - f(u^*(x, t)) + r(x, t)) dx \\ (3.25) \quad &=: I(t) + J(t). \end{aligned}$$

Because $u_{\theta_t}(\cdot)|_{\partial\Omega} = u^*(\cdot, t)|_{\partial\Omega} = 0$, we know $\delta(\cdot, t)|_{\partial\Omega} = 0$. Thus, we have

$$\begin{aligned} I(t) &= \int_\Omega \delta(x, t) (\nabla \cdot (A(x) \nabla \delta(x, t)) + b(x) \cdot \nabla \delta(x, t)) dx \\ (3.26) \quad &= - \int_\Omega \nabla \delta(x, t)^\top A(x) \nabla \delta(x, t) dx - \frac{1}{2} \int_\Omega (\nabla \cdot b(x)) \delta(x, t)^2 dx \\ &\leq -\lambda \int_\Omega |\nabla \delta(x, t)|^2 dx - \frac{1}{2} \int_\Omega (\nabla \cdot b(x)) \delta(x, t)^2 dx \\ &\leq -\frac{\lambda}{C_p} \int_\Omega |\delta(x, t)|^2 dx + \frac{B}{2} \int_\Omega |\delta(x, t)|^2 dx, \end{aligned}$$

where the first equality is just by the definition of $I(t)$, the second equality is obtained by integrating by parts on both terms and using $\delta(\cdot, t)|_{\partial\Omega} = 0$, the first inequality is due to (3.20), and the last inequality is due to the Poincaré's inequality

$$\|\delta(\cdot, t)\|_2 \leq C_p \|\nabla \delta(\cdot, t)\|_2$$

as $\delta(\cdot, t)|_{\partial\Omega} = 0$ for all t (here C_p the Poincaré's constant depending on Ω only) and the bound (3.21). We can also obtain

$$\begin{aligned}
 J(t) &= \int_{\Omega} \delta(x, t) (f(u_{\theta_t}(x)) - f(u^*(x, t)) - r(x, t)) dx \\
 &\leq \int_{\Omega} |\delta(x, t)| \cdot |f(u_{\theta_t}(x)) - f(u^*(x, t)) - r(x, t)| dx \\
 (3.27) \quad &\leq \int_{\Omega} |\delta(x, t)| \cdot (L_f |\delta(x, t)| + |r(x, t)|) dx \\
 &\leq L_f \|\delta(x, t)\|_2^2 + \|r(\cdot, t)\|_2 \|\delta(\cdot, t)\|_2 \\
 &\leq L_f \|\delta(x, t)\|_2^2 + \varepsilon \|\delta(\cdot, t)\|_2,
 \end{aligned}$$

where the first identity is by the definition of $J(t)$, the second inequality is due to the Lipschitz condition of f . Combining (3.24), (3.25), (3.26) and (3.27), we obtain

$$D'(t) \leq \left(L_f + \frac{B}{2} - \frac{\lambda}{C_p} \right) D(t) + |\Omega|^{1/2} \varepsilon.$$

By Grönwall's inequality we deduce that

$$D(t) \leq e^{(L_f + B/2 - \lambda/C_p)t} (D(0) + |\Omega|^{1/2} \varepsilon t).$$

Recall that

$$D(0) = \|\delta(\cdot, 0)\|_2 = \|u_{\theta_0}(\cdot) - u^*(\cdot, 0)\|_2 = \|u_{\theta_0}(\cdot) - g(\cdot)\|_2 \leq \varepsilon_0,$$

we thus have

$$\|u(\cdot, \theta(t)) - u(\cdot, t)\|_2 = D(t) \leq e^{(L_f + B/2 - \lambda/C_p)t} (\varepsilon_0 + \varepsilon t)$$

for all time t , which completes the proof. \square

Remark 3.6. While we assumed f to be globally Lipschitz, the result in Theorem 3.5 still holds locally with local Lipschitz condition of f . For example, in the case of the Allen-Cahn example, we know if our initial function is bounded by 1 the true trajectories will remain bounded allowing the results of Theorem 3.5 to apply.

COROLLARY 3.7. *Suppose the conditions in Theorem 3.5 hold. Let $\hat{\theta}_t$ be the numerical solution to the ODE (3.9) obtained by using the Euler scheme with step size $h > 0$. Then*

$$(3.28) \quad \|u_{\hat{\theta}_t}(\cdot) - u^*(\cdot, t)\|_2 \leq \frac{L_V M_V |\Omega| h}{2} (e^{L_V t} - 1) + e^{(L_f - B/2 + \eta/C_p)t} (\varepsilon_0 + \bar{\varepsilon} t)$$

for all t as long as $\theta_t \in \bar{\Theta}$.

Proof. Given the estimate provided in Theorem 3.5, we only need to show

$$(3.29) \quad \|u_{\hat{\theta}_t}(\cdot) - u_{\theta_t}(\cdot)\|_2 \leq \frac{L_V M_V |\Omega| h}{2} (e^{L_V t} - 1),$$

since combined with (3.23) it yields the claimed estimate (3.28). To show (3.29), we notice that

$$\ddot{\theta}_t = \frac{d}{dt} V_{\xi}(\theta_t) = \nabla_{\theta} V_{\xi}(\theta_t) \cdot \dot{\theta}_t = \nabla_{\theta} V_{\xi}(\theta_t) \cdot V_{\xi}(\theta_t).$$

Therefore we have

$$|\ddot{\theta}_t| = |\nabla_{\theta} V_{\xi}(\theta_t) \cdot V_{\xi}(\theta_t)| \leq L_V M_V$$

where L_V and M_V are defined in (3.22). Hence, by the standard results for the Euler's method [4, pp. 346], we know the numerical solution $\hat{\theta}_t$ satisfies

$$(3.30) \quad |\hat{\theta}_t - \theta_t| \leq \frac{h M_V}{2} (e^{L_V t} - 1)$$

for all t . Therefore, we obtain

$$\begin{aligned} \|u_{\hat{\theta}_t} - u_{\theta_t}\|_2 &= \left(\int_{\Omega} |u_{\hat{\theta}_t}(x) - u_{\theta_t}(x)|^2 dx \right)^{1/2} = \left(\int_{\Omega} |\nabla_{\theta} u_{\hat{\theta}_t}(x) \cdot (\hat{\theta}_t - \theta_t)|^2 dx \right)^{1/2} \\ &\leq L_V |\Omega| |\hat{\theta}_t - \theta_t| \leq \frac{L_V M_V |\Omega| h}{2} (e^{L_V t} - 1), \end{aligned}$$

where the second equality is due to the fact that u_{θ} is C^1 in θ and hence the mean value theorem applies to u_{θ} (here $\hat{\theta}_t$ is some point on the line segment between $\hat{\theta}_t$ and θ_t). \square

The proof above can be modified if a different numerical ODE solver is employed. In that case one can obtain improved upper bound and order in step size h in (3.30).

4. Numerical Results.

4.1. Implementation of the training process of control field V_{ξ} . In Section 3.2, we have showed that the neural control field V_{ξ} is parameterized as a deep network, and its parameter ξ can be learned by solving

$$\min_{\xi} \left\{ \ell(\xi) := \int_{\Theta} \|V_{\xi}(\theta) \cdot \nabla_{\theta} u_{\theta} - F[u_{\theta}]\|_2^2 d\theta \right\}.$$

The first-order optimality condition of this minimization problem is given by $G(\theta)V_{\xi}(\theta) = p(\theta)$ where $G(\theta)$ and $p(\theta)$ are defined in (3.17). The objective function $\ell(\xi)$ above shares the same minimizers as the following one:

$$(4.1) \quad \bar{\ell}(\xi) := \int_{\Theta} |G(\theta)V_{\xi}(\theta) - p(\theta)|^2 d\theta.$$

In our numerical experiments, we use $\bar{\ell}$ defined in (4.1) as the loss function where $p(\theta)$ already represents the projection of $F[u_{\theta}]$ onto the $T_{u_{\theta}}\mathcal{M}$ space and it yields better performance empirically. Moreover, we know the minimum loss value of (4.1) is 0, which contrasts to (3.10) where the minimum loss value is often unknown.

In practice, as the dimension of θ and Ω could be large, we have to approximate (4.1) using techniques such as Monte-Carlo integration. This leads to the approximate forms

$$\tilde{G}(\theta) = \frac{1}{N_x} \sum_{i=1}^{N_x} \nabla_{\theta} u_{\theta}(x_i) \nabla_{\theta} u_{\theta}(x_i)^{\top}, \quad \tilde{p}(\theta) = \frac{1}{N_x} \sum_{i=1}^{N_x} \nabla_{\theta} u_{\theta}(x_i) F[u_{\theta}](x_i),$$

where $x_i, i = 1, \dots, N_x$ are sampled from Ω . By also drawing samples from Θ , we arrive at our empirical loss function defined by

$$(4.2) \quad \ell_1(\xi) := \frac{1}{N_{\theta}} \sum_{j=1}^{N_{\theta}} |\tilde{G}(\theta_j) \cdot V_{\xi}(\theta_j) - \tilde{p}(\theta_j)|^2.$$

To improve the training of V_{ξ} , we also augment the loss function ℓ_1 in (4.2) with an additional term following a data-driven approach. Specifically, we follow the methods in [10, 19] to generate multiple sample trajectories starting from randomly sampled initial values $\{\theta_0^{(i)} : i \in [M]\}$ in Θ . For the i th trajectory, a sequence of directions $\{v_j^{(i)} : j = 0, 1, \dots, N_t\}$ are solved from linear systems $\tilde{G}(\theta_j^{(i)})v_j^{(i)} = \tilde{p}(\theta_j^{(i)})$ and the discrete-time points on the trajectory are obtained by $\theta_{j+1}^{(i)} = \theta_j^{(i)} + h v_j^{(i)}$ for $j = 0, 1, \dots, N_t - 1$. We add the augment loss term

$$(4.3) \quad \ell_2(\xi) := \frac{1}{N_t M} \sum_{i=1}^M \sum_{j=1}^{N_t} |V_{\xi}(\theta_j^{(i)}) - v_j^{(i)}|^2.$$

Combining with (4.2), we obtain our final loss function

$$(4.4) \quad \ell_{\text{total}}(\xi) = \ell_1(\xi) + \zeta \ell_2(\xi),$$

where ζ is a weight parameter. In our experience for parabolic linear PDEs using only ℓ_1 is sufficient to generate a good result. For the nonlinear case adding ℓ_2 substantially improves training results empirically as network parameters may move far away from those we sampled near the initial parameters.

4.2. Experimental setting. To demonstrate the performance of the proposed method, we test it on three different PDEs: a 10-dimensional (10D) transport equation, a 10D heat equation, and a 2D Allen-Cahn equation. Both of the transport equation and heat equation are linear PDEs, while the Allen-Cahn is a highly nonlinear PDE. In fact, we also tested 10D Allen-Cahn equation but only present the result of the 2D one here. This is because the true solution of Allen-Cahn equation does not have closed-form, and we have to employ a classical finite difference method, which does not scale to 10D case, to produce a reference solution for comparison. In contrast, we have closed-form solutions of the IVPs with transport and heat equations and hence we can use them as the true solution for direct comparison. In our tests, we employ the following structure of our reduced-order model

$$(4.5) \quad u_\theta(x) = \alpha(x)z_L(x, \theta)$$

for the heat equation and Allen-Cahn equation. We use the following network structure

$$(4.6) \quad u_\theta(x) = z_L(\beta(x), \theta)$$

for the transport equation. In (4.5), $\alpha(x)$ is a distance function of $\partial\Omega$ such that it satisfies the zero boundary condition, and in (4.6) $\beta(x)$ is a function chosen to satisfy a periodic boundary condition as in [19]. This aligns with our choice of u_θ in (4.5) and (4.6) as the IVP with heat and Allen-Cahn equations have zero boundary value whereas the IVP with transport equation has periodic boundary value in our experiments. In both (4.5) and (4.6), z_L is the neural network and is defined by

$$(4.7) \quad z_L = w_L z_{L-1}, \quad z_l = z_{l-1} + \sigma(W_l z_{l-1} + b_l), \quad l = 1, \dots, L-1$$

and $z_0 = \sigma(W_0 x + b_0)$. Here σ is a user-chosen activation function (we use tanh in our experiments) $W_l \in \mathbb{R}^{d' \times d'}$ are the weight vectors and $b_l \in \mathbb{R}^{d'}$ are the bias vectors, and $W_0 \in \mathbb{R}^{d' \times d}$ and $w_L \in \mathbb{R}^{1 \times d}$, all of these matrices and vectors make up the parameter vector θ . Networks such as in (4.7) are often called *residual neural networks* (ResNet), and have been shown performing better than basic feed forward networks in function approximation [73]. The values of L and d' in our experiments are shown in Table 1. They are selected manually to balance the depth L and width d' so that u_θ does not have too many neurons but still remains expressive. We do the same for the vector field V_ξ , using the structure (4.7) with tanh activation. The width and depth of this network are also collected in Table 1.

Information about the number of trajectories used for (4.3) is also collected in Table 1. For all of the experiments, we set the weight $\zeta = 0.1$ in (4.4) to reflect the scale difference of the two loss terms and use the standard ADAM optimizer with learning rate 0.001, $\beta_1 = 0.9$, $\beta_2 = 0.999$. We terminate the training process when the empirical loss $\ell_{\text{total}}(\xi) < 0.1$. Once V_ξ is learned, we use the 4th-order Runge-Kutta method with a step size of $T/200$ (T is determined from the problem) to solve θ_t from the ODE in (3.9) in Algorithm 3.2 and compare the corresponding u_θ with the reference solutions. All the implementations and experiments are performed using PyTorch in Python 3.9 in Windows 10 OS on a desktop computer with an AMD Ryzen 7 3800X 8-Core Processor at 3.90 GHz, 16 GB of system memory, and an Nvidia GeForce RTX 2080 Super GPU with 8 GB of graphics memory.

Finally, we note the process for designing Θ . In our experiments, the following process was used: We first considered a few different initial conditions that we were interested to test for a particular IVP. These initials were chosen to either give us analytical examples to compare against when we later tested our model or because they represented some common test examples to compare against. Then we trained u_θ to approximate those initial conditions gaining some relevant $\theta_0 \in \mathbb{R}^m$ by training as in step 1 of Algorithm 3.2 for error tolerance 10^{-4} . In practice, a user may have some class of functions they wish to be able to test around, and locating what region of Θ corresponds to approximations of our desired initials would then become an important design step. As neural networks can be expressive and Θ large, using too much of the parameter space becomes computationally difficult, while also including many examples we may not care about.

Once found, we use the θ_0 's to design Θ as the union of radius 3 balls centered at each initial. We then can randomly sample from these balls to form our training sets. It is worth noting, that our method of creating Θ is a potential challenge in using this method. Designing Θ to be large enough to remain relevant to the initials one wants to be able to rapidly test, while not so large as to make approximating the control vector field too challenging, is a difficult balance to strike. Indeed, it is not hard to see that this problem

Table 1: The considered dimensions of the three toy problems as well as the network dimension considered and the number of training trajectories/samples. Here M is the number of trajectories used from Θ and N_θ is the total number of samples from Θ .

Problem	Dim.	u_θ Width/Depth	V_ξ Width/Depth	M	N_θ
Heat Equation	10	12/4	1,500/4	2,000	600,000
Transport Equation	10	12/4	500/5	2,000	450,000
Allen-Cahn Equation	2	6/3	800/3	1,600	200,000

is highly dependent upon the type of reduced order model one wishes to use, as well as the PDE structure. As of now, we do not have a clear answer on the best way to approach designing Θ for arbitrary neural networks. This poses an interesting avenue for future research, but we do not consider it here.

4.3. Numerical results on transport equation. We first consider the initial value problem defined by a 10D transport equation with periodic boundary conditions as follows:

$$(4.8) \quad \begin{cases} \partial_t u(x, t) = -\mathbf{1} \cdot \nabla_x u(x, t), & \forall x \in \Omega, t \in [0, T], \\ u(x, 0) = g(x), & \forall x \in \bar{\Omega}, \end{cases}$$

where $\Omega = (0, 1)^{10}$, $T = 1$, $\mathbf{1}$ is the vector whose components are all ones, and the boundary value $u(x, t) = 0$ for all $x \in \partial\Omega$ and $t \in [0, T]$. This IVP has the true solution $u^*(x, t) = g(x - \mathbf{1} \cdot t)$. We obtain the solution operator of the IVP (4.8), we use (4.6) as the reduced-order model u_θ and define $\beta(x) = (\cos(2\pi(x - b)), \sin(2\pi(x - b)))^\top$ where $b \in \mathbb{R}^{10}$ is a trainable parameter with sin and cos acting component-wise to x . This means that the first hidden layer uses $W_0 \in \mathbb{R}^{12 \times 20}$. Then we train the neural control vector field V_ξ by minimizing (3.10) with the number of sampled θ in Θ shown in Table 1.

After the control V_ξ is obtained, we test the performance of neural control of the parameter θ of u_θ using V_ξ on a variety of initial values g for the IVP (4.8). Due to space limitation, we only plot the results of the solutions for perturbations of the following three initial values:

$$(4.9) \quad \begin{aligned} g_1(x) &= \sin(2\pi x_1) \sin(2\pi x_2) \prod_{i=3}^{10} \sin(\pi x_i), \\ g_2(x) &= \sin(2\pi x_1) \cos(2\pi x_2) \prod_{i=3}^{10} \sin(\pi x_i), \\ g_3(x) &= \sin(4\pi x_1) \sin(2\pi x_2) \prod_{i=3}^{10} \sin(\pi x_i). \end{aligned}$$

We emphasize that the corresponding θ_0 's to these initial values are not specifically used in the training process. In order to evaluate the generalization ability of the proposed approach we approximate solutions to the IVP using initial values $\theta_0 + \delta$ where $\delta \in \mathbb{R}^m$ and $|\delta| = 1$ is determined randomly. These approximate solutions are shown in Figure 1. For g_1 , we plot the corresponding true solution $u^*(\cdot, t)$ using the perturbation as the initial, the approximate solution u_{θ_t} obtained by Algorithm 3.2, and their pointwise absolute difference $|u_{\theta_t}(x) - u^*(x, t)|$ from row 1 to row 3 in Figure 1 respectively for $t = 0, 0.15, 0.5, 0.85, 1$. The plots for g_2 and g_3 are shown in rows 4–6 and 7–9 in Figure 1 respectively. We only show the cross sections of the x_1 - x_2 plane for these plots as they have the largest variations in the solution. From Figure 1, we can see that the reduced-order model u_{θ_t} with θ_t controlled by the trained vector field V_ξ closely approximates the true solution $u^*(\cdot, t)$ with low absolute errors (we'd like to point out that the scale of the error is different from that of $u^*(\cdot, t)$ and $u_{\theta_t}(\cdot)$). The plot of $\|u_\theta - u^*(\cdot, t)\|_2 / \|u^*(\cdot, t)\|_2$ vs t seen in Figure 2 further justifies the small approximation error using the proposed method.

4.4. Heat equation. Next we consider an initial value problem with heat equation in 10D:

$$(4.10) \quad \begin{cases} \partial_t u(x, t) = \Delta u(x, t), & \forall x \in \Omega, t \in [0, T] \\ u(x, 0) = g(x), & \forall x \in \bar{\Omega}, \end{cases}$$

where $\Omega = (0, 1)^{10}$ and the boundary value $u(x, t) = 0$ for all $x \in \partial\Omega$ and $t \in [0, T]$. As most of the initial conditions we consider have rapid evolution in a short time, we use $T = 0.015$ in this test. For neural network we use (4.5), with $\alpha(x) = \prod_{i=1}^{10} 4(x_i - x_i^2)$.

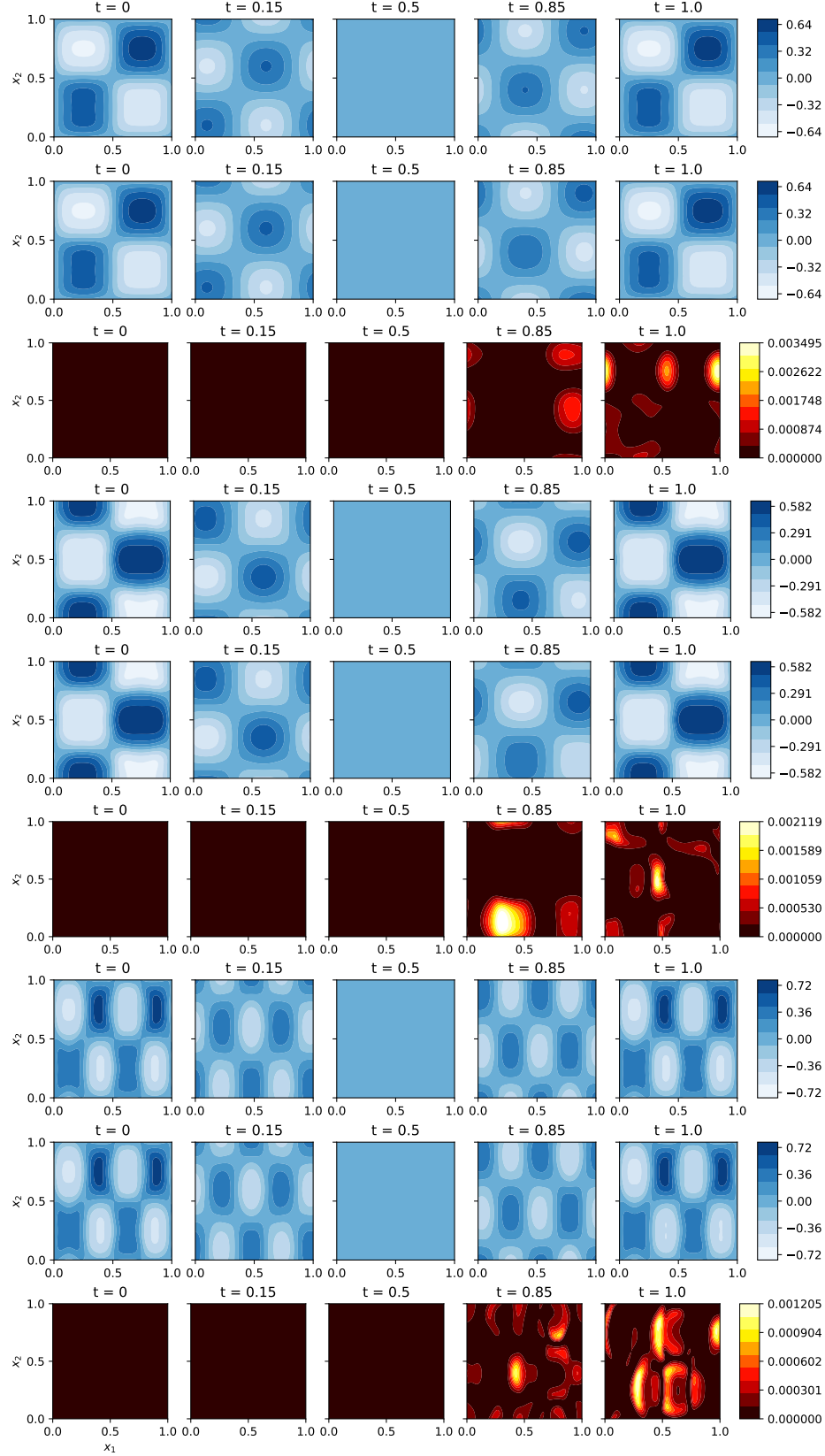


Fig. 1: (Transport equation). Comparison between true solution $u^*(\cdot, t)$, the approximation $u_{\theta_t}(\cdot)$ and their pointwise absolute difference $|u_{\theta_t}(x) - u^*(x, t)|$ for times $t = 0, 0.15, 0.5, 0.85, 1$ for IVPs with initial values g_1 (rows 1–3), g_2 (rows 4–6) and g_3 (rows 7–9) which are given in (4.9).

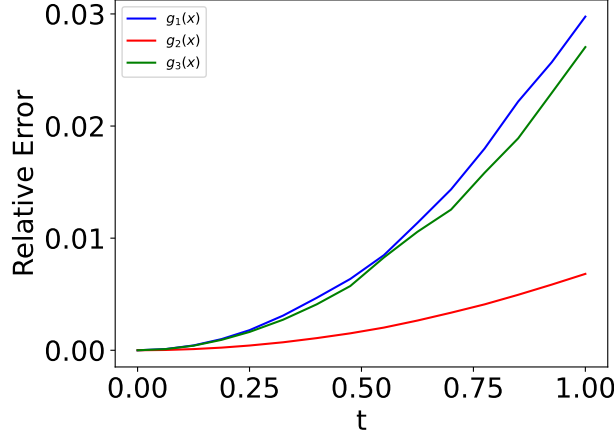


Fig. 2: (Transport equation). Comparison of the relative error $\|u^*(\cdot, t) - u_{\theta_t}(\cdot)\|_2 / \|u^*(\cdot, t)\|_2$ over time t for IVPs with initial values perturbed near g_1 , g_2 and g_3 which are given in (4.9).

Again due to space limitation, we only demonstrate the performance on three initial conditions with analytical solutions whose corresponding θ_0 parameters were not contained in the training data. These initial conditions are given by

$$\begin{aligned}
 (4.11) \quad g_1(x) &= \sin(2\pi x_1) \sin(2\pi x_2) \prod_{i=3}^{10} \sin(\pi x_i) + 0.5 \prod_{i=1}^{10} \sin(\pi x_i), \\
 g_2(x) &= \sin(2\pi x_1) \sin(2\pi x_2) \prod_{i=3}^{10} \sin(\pi x_i), \\
 g_3(x) &= \sin(2\pi x_1) \prod_{i=2}^{10} \sin(\pi x_i).
 \end{aligned}$$

We chose these three initials because they yield solutions with closed-form expressions as follows:

$$\begin{aligned}
 (4.12) \quad u_1^*(x, t) &= e^{-16\pi^2 t} \sin(2\pi x_1) \sin(2\pi x_2) \prod_{i=3}^{10} \sin(\pi x_i) + 0.5 e^{-10\pi^2 t} \prod_{i=1}^{10} \sin(\pi x_i), \\
 u_2^*(x, t) &= e^{-16\pi^2 t} \sin(2\pi x_1) \sin(2\pi x_2) \prod_{i=3}^{10} \sin(\pi x_i), \\
 u_3^*(x, t) &= e^{-13\pi^2 t} \sin(2\pi x_1) \prod_{i=2}^{10} \sin(\pi x_i),
 \end{aligned}$$

The short time scale is used as for larger T the solutions decay towards 0. From Figures 3 and 4, we observe that the proposed method can quickly approximate the true solutions with consistently low relative error up to 3%.

4.5. Allen-Cahn equation. In this test, we consider the IVP with nonlinear Allen-Cahn equation given by

$$(4.13) \quad \begin{cases} \partial_t u(x, t) = \epsilon \Delta u(x, t) + \frac{3}{2} (u(x, t) - u(x, t)^3), & \forall x \in \Omega, t \in (0, T] \\ u(x, 0) = g(x), & \forall x \in \bar{\Omega}, \end{cases}$$

where $\Omega = (0, 1)^2$, $\epsilon = 0.0001$, and the boundary value $u(x, t) = 0$ for all $x \in \partial\Omega$ and $t \in [0, T]$. As the Allen-Cahn PDE does not have analytical solution to compare against, we have to resort to the classical finite difference method to generate a reference solution for comparison in 2D case only, despite that our method can be applied to higher dimensional case. In this test, we again use (4.5) with $\alpha(x) = 4^2(x_1 - x_1^2)(x_2 - x_2^2)$ as our neural network. For comparison we use the following initial conditions:

$$\begin{aligned}
 (4.14) \quad g_1(x) &= 0.75 \sin(3\pi x_1) \sin(\pi x_2) \\
 g_2(x) &= (x_1 - x_1^2) \cos(2\pi x_1) \sin(\pi x_2) \\
 g_3(x) &= (x_1 - x_1^2) \cos(2\pi x_1) \sin(2\pi x_2).
 \end{aligned}$$

Note that we excluded these initials during the training of V_ξ to test the generalization property of the proposed method. The results of the proposed method at time $t = 0, 0.15, 0.3, 0.45, 0.6$ are shown in Figure 6. Again, the plots for g_1 are in rows 1–3, while the plots for g_2 and g_3 are shown in rows 4–6 and 7–9 in Figure 6 respectively. In Figure 5 we compare the relative error $\|u_{\theta_t} - u^*(\cdot, t)\|_2 / \|u^*(\cdot, t)\|_2$ against the time t . We again observe promising approximation accuracy using the proposed method in these figures. In Figure 5 we see how the g_1 initial value increases faster than the other solutions because the solution to the Allen-Cahn equation for this initial value has fast increasing derivatives as time progresses, which poses a challenge to all numerical methods including ours in solving Allen-Cahn equations in general. Specifically, such large derivatives force the parameter θ of the neural network to blow up quickly, and hence the trajectory θ_t may rapidly escape from the prescribed Θ over which we trained the vector field V_ξ . This is a challenge that remains to be overcome using more adaptive training method and sampling strategy.

5. Variations and Generalizations. In this section, we discuss potential variations and generalizations of the proposed approach. Specifically, one can modify the proposed method such that it applies to general time-dependent evolution PDEs. IVP with boundary value conditions are also addressed.

Applications to general time-dependent PDEs. Our approach can be readily applied to a large variety of time-dependent PDEs. The key reason is that these PDEs can be converted to the exact form of (3.5) for which our method is designed. To avoid overloading the bracket notation, we temporarily use $F(u)$ and $F(t, u)$ to represent $F[u]$ and $F_t[u]$ (differential operator that explicitly depends on time t) in this paragraph. Then we may convert any non-autonomous evolution PDE into an autonomous one:

$$(5.1) \quad \partial_t u = F(t, u) \iff \partial_t u = \tilde{F}(u), \text{ where } u := [t; u], \tilde{F}(u) := [1; F(u)],$$

and $[\cdot; \cdot]$ means to stack the two arguments vertically to form a single one. Therefore, our approach can be easily modified to tackle non-autonomous PDEs due to (5.1). Similarly, we can consider equations with higher order time derivatives such as wave equations by converting them to the standard evolution PDE with first-order time derivative:

$$(5.2) \quad \partial_{tt} u = F(u) \iff \partial_t u = \tilde{F}(u), \text{ where } u := [u; v], \tilde{F}(u) := [v; F(u)].$$

History-dependent PDEs can also be considered: denote $H_u(t) := \{u(\cdot, s) \mid 0 \leq s \leq t\}$ the trajectory recording the path of u up to time t and F a nonlinear operator on path H_u , then we can set $H_u(t)$ as an auxiliary variable and convert the problem $\partial_t u = F[H_u]$ to an autonomous evolution PDE of $[u; H_u]$.

Evolution PDEs with boundary conditions. In many real-world applications, IVP may also be associated with boundary conditions. We can extend our method to handle this situation. Let ϕ denote any boundary value function for the IVP. Therefore, in addition to the evolution PDE and initial value, the solution u must also satisfy the boundary condition $u(x, t) = \phi(x, t)$ for all $x \in \partial\Omega$ and $t \in [0, T]$. To cope with this requirement, we propose to parameterize the solution of the IVP as $u_\theta(x) = \varphi_\eta(x) + \alpha(x)\psi_\zeta(x)$ with parameter $\theta = (\eta, \zeta)$, where φ_η and ψ_ζ are two reduced-order models with parameters η and ζ , respectively, and $\alpha(x)$ is a prescribed smooth function such that $\alpha(x) > 0$ if $x \in \Omega$ and $\alpha(x) = 0$ if $x \in \partial\Omega$ (such α function is easy to construct in practice). The purpose of φ_η is to fit the given boundary value ϕ , which is not interfered by $\alpha\psi_\zeta$ because the latter vanishes at the boundary $\partial\Omega$. Following our approach discussed in 3.2, we can again form a control vector field $V_\xi(\theta) = V_\xi(\eta, \zeta)$. Here the parameter η_t plays two roles: it enforces φ_{η_t} to fit the boundary condition $\phi(\cdot, t)$ on $\partial\Omega$ and serves together with ζ_t as the control input to the vector field V_ξ so that u_{θ_t} minimizes the projection error given in (3.10).

6. Conclusion and Future Work. We have shown a novel strategy for solving linear and nonlinear evolution PDEs numerically. Specifically, we propose to use deep neural networks as nonlinear reduced-order models to represent PDE solutions, and learn a control vector field to steer the network parameter so that the induced time-evolving neural network can approximate the solution accurately. The proposed method allows a user to quickly solve an evolution PDE with different initial values without the need to retrain the neural network. Error estimates of the proposed approach are also provided.

We implemented the nonlinear reduced-order models as generic deep networks which yield promising results. We expect that the accuracy and effectiveness can be further improved by incorporating structural information and prior knowledge about the PDE and its solutions into the design of these networks. Training of control vector fields can also be made more efficient by integrating informative sample trajectories of θ_t .

These improvements can potentially make the proposed method very effective in solving evolution PDEs in specified application domains.

REFERENCES

- [1] W. F. Ames. *Numerical methods for partial differential equations*. Academic press, 2014.
- [2] W. Anderson and M. Farazmand. Evolution of nonlinear reduced-order solutions for pdes with conserved quantities. *SIAM Journal on Scientific Computing*, 44(1):A176–A197, 2022.
- [3] C. Anitescu, E. Atroshchenko, N. Alajlan, and T. Rabczuk. Artificial neural network methods for the solution of second order boundary value problems. *Computers, Materials & Continua*, 59(1):345–359, 2019.
- [4] K. Atkinson. *An Introduction to Numerical Analysis (2nd ed.)*. John Wiley I& Sons, 1989.
- [5] G. Bao, X. Ye, Y. Zang, and H. Zhou. Numerical solution of inverse problems by weak adversarial networks. *Inverse Problems*, 36(11):115003, 2020.
- [6] C. Beck, W. E, and A. Jentzen. Machine learning approximation algorithms for high-dimensional fully nonlinear partial differential equations and second-order backward stochastic differential equations. *Journal of Nonlinear Science*, pages 1–57, 2017.
- [7] J. Berg and K. Nyström. A unified deep artificial neural network approach to partial differential equations in complex geometries. *Neurocomputing*, 317:28–41, 2018.
- [8] N. Boullé, C. Earls, and A. Townsend. Data-driven discovery of green’s functions with human-understandable deep learning. *Scientific Reports*, 12:4824, 03 2022.
- [9] N. Boullé, S. Kim, T. Shi, and A. Townsend. Learning green’s functions associated with time-dependent partial differential equations. *Journal of Machine Learning Research*, 23:1–34, 08 2022.
- [10] J. Bruna, B. Pherstorfer, and E. Vanden-Eijnden. Neural galerkin scheme with active learning for high-dimensional evolution equations. *arXiv preprint arXiv:2203.01360*, 2022.
- [11] S. Cai, Z. Wang, L. Lu, T. A. Zaki, and G. E. Karniadakis. Deepm&mnet: Inferring the electroconvection multiphysics fields based on operator approximation by neural networks. *arXiv preprint arXiv:2009.12935*, 2020.
- [12] W. Cai, X. Li, and L. Liu. A phase shift deep neural network for high frequency approximation and wave problems. *SIAM Journal on Scientific Computing*, 42(5):A3285–A3312, 2020.
- [13] W. Cai and Z.-Q. J. Xu. Multi-scale deep neural networks for solving high dimensional pdes. *arXiv preprint arXiv:1910.11710*, 2019.
- [14] Y. Chen, B. Dong, and J. Xu. Meta-mgnet: Meta multigrid networks for solving parameterized partial differential equations. *arXiv preprint arXiv:2010.14088*, 2020.
- [15] P. Clark Di Leoni, C. Meneveau, G. Karniadakis, and T. Zaki. Deep operator neural networks (deeponets) for prediction of instability waves in high-speed boundary layers. *Bulletin of the American Physical Society*, 2020.
- [16] S. Cuomo, V. S. Di Cola, F. Giampaolo, G. Rozza, M. Raissi, and F. Piccialli. Scientific machine learning through physics-informed neural networks: Where we are and what’s next. *arXiv preprint arXiv:2201.05624*, 2022.
- [17] M. Dissanayake and N. Phan-Thien. Neural-network-based approximations for solving partial differential equations. *Communications in Numerical Methods in Engineering*, 10(3):195–201, 1994.
- [18] S. Dong and N. Ni. A method for representing periodic functions and enforcing exactly periodic boundary conditions with deep neural networks. *arXiv preprint arXiv:2007.07442*, 2020.
- [19] Y. Du and T. A. Zaki. Evolutional deep neural network. *Phys. Rev. E*, 104:045303, Oct 2021.
- [20] W. E, J. Han, and A. Jentzen. Deep learning-based numerical methods for high-dimensional parabolic partial differential equations and backward stochastic differential equations. *arXiv preprint arXiv:1706.04702*, 5(4):349–380, 2017.
- [21] W. E and B. Yu. The deep ritz method: a deep learning-based numerical algorithm for solving variational problems. *Communications in Mathematics and Statistics*, 6(1):1–12, 2018.
- [22] G. Evans, J. Blackledge, and P. Yardley. *Numerical methods for partial differential equations*. Springer Science & Business Media, 2012.
- [23] L. C. Evans. *Partial differential equations*, volume 19 of *Graduate Studies in Mathematics*. American Mathematical Society, Providence, RI, 1998.
- [24] Y. Fan, C. O. Bohorquez, and L. Ying. Bcr-net: A neural network based on the nonstandard wavelet form. *Journal of Computational Physics*, 384:1–15, 2019.
- [25] M. Fujii, A. Takahashi, and M. Takahashi. Asymptotic expansion as prior knowledge in deep learning method for high dimensional bsdes. *Asia-Pacific Financial Markets*, pages 1–18, 2017.
- [26] Y. Gu, C. Wang, and H. Yang. Structure probing neural network deflation. *arXiv preprint arXiv:2007.03609*, 2020.
- [27] Y. Gu, H. Yang, and C. Zhou. Selectnet: Self-paced learning for high-dimensional partial differential equations. *arXiv preprint arXiv:2001.04860*, 2020.
- [28] I. Guhring, G. Kutyniok, and P. Peterson. Error bounds for approximations with deep relu neural networks in $w^{s,p}$ norms. *Analysis and Applications*, 18:803–859, 2020.
- [29] I. Guhring and M. Raslan. Approximation rates for neural networks with encodable weights in smoothness spaces. *Neural Networks*, 134:107–130, 11 2020.
- [30] J. Han, A. Jentzen, and W. E. Overcoming the curse of dimensionality: Solving high-dimensional partial differential equations using deep learning. *arXiv preprint arXiv:1707.02568*, pages 1–13, 2017.
- [31] J. Han, A. Jentzen, and W. E. Solving high-dimensional partial differential equations using deep learning. *Proceedings of the National Academy of Sciences*, 115(34):8505–8510, 2018.
- [32] J. Han, J. Lu, and M. Zhou. Solving high-dimensional eigenvalue problems using deep neural networks: A diffusion monte carlo like approach. *Journal of Computational Physics*, 423:109792, 2020.
- [33] Y. Han, J. Yoo, H. H. Kim, H. J. Shin, K. Sung, and J. C. Ye. Deep learning with domain adaptation for accelerated

- projection-reconstruction mr. *Magnetic resonance in medicine*, 80(3):1189–1205, 2018.
- [34] K. Hornik. Approximation capabilities of multilayer feedforward networks. *Neural networks*, 4(2):251–257, 1991.
 - [35] K. Hornik, M. Stinchcombe, and H. White. Multilayer feedforward networks are universal approximators. *Neural networks*, 2(5):359–366, 1989.
 - [36] J. Huang, H. Wang, and H. Yang. Int-deep: A deep learning initialized iterative method for nonlinear problems. *Journal of Computational Physics*, 419:109675, 2020.
 - [37] C. Huré, H. Pham, and X. Warin. Deep backward schemes for high-dimensional nonlinear pdes. *Mathematics of Computation*, 89(324):1547–1579, 2020.
 - [38] M. Hutzenthaler, A. Jentzen, T. Kruse, and T. A. Nguyen. A proof that rectified deep neural networks overcome the curse of dimensionality in the numerical approximation of semilinear heat equations. *SN partial differential equations and applications*, 1(2):1–34, 2020.
 - [39] A. D. Jagtap, K. Kawaguchi, and G. E. Karniadakis. Adaptive activation functions accelerate convergence in deep and physics-informed neural networks. *Journal of Computational Physics*, 404:109136, 2020.
 - [40] C. Johnson. *Numerical solution of partial differential equations by the finite element method*. Courier Corporation, 2012.
 - [41] E. Kharazmi, Z. Zhang, and G. E. Karniadakis. hp-vpinns: Variational physics-informed neural networks with domain decomposition. *arXiv preprint arXiv:2003.05385*, 2020.
 - [42] N. Kovachki, S. Lanthaler, and S. Mishra. On universal approximation and error bounds for fourier neural operators. *Journal of Machine Learning Research*, 22:Art–No, 2021.
 - [43] M. Kumar and N. Yadav. Multilayer perceptrons and radial basis function neural network methods for the solution of differential equations: a survey. *Computers & Mathematics with Applications*, 62(10):3796–3811, 2011.
 - [44] I. E. Lagaris, A. Likas, and D. I. Fotiadis. Artificial neural networks for solving ordinary and partial differential equations. *IEEE transactions on neural networks*, 9(5):987–1000, 1998.
 - [45] H. Lee and I. S. Kang. Neural algorithm for solving differential equations. *Journal of Computational Physics*, 91(1):110–131, 1990.
 - [46] B. Li, S. Tang, and H. Yu. Better approximations of high dimensional smooth functions by deep neural networks with rectified power units. *Communications in Computational Physics*, 27:379–411, 02 2020.
 - [47] Z. Li, N. Kovachki, K. Azizzadenesheli, B. Liu, K. Bhattacharya, A. Stuart, and A. Anandkumar. Fourier neural operator for parametric partial differential equations. *arXiv preprint arXiv:2010.08895*, 2020.
 - [48] Z. Li, N. Kovachki, K. Azizzadenesheli, B. Liu, K. Bhattacharya, A. Stuart, and A. Anandkumar. Neural operator: Graph kernel network for partial differential equations. *arXiv preprint arXiv:2003.03485*, 2020.
 - [49] S. Liang and R. Srikant. Why deep neural networks for function approximation? In *International Conference on Learning Representations (ICLR)*, 2017.
 - [50] S. Liang and H. Yang. Finite expression method for solving high-dimensional partial differential equations. *arXiv preprint arXiv:2206.10121*, 2022.
 - [51] G. Lin, F. Chen, P. Hu, X. Chen, J. Chen, J. Wang, and Z. Shi. Bi-greenet: Learning green’s functions by boundary integral network. *arXiv preprint arXiv:2204.13247*, 2022.
 - [52] Z. Liu, W. Cai, and Z.-Q. J. Xu. Multi-scale deep neural network (mscalednn) for solving poisson-boltzmann equation in complex domains. *arXiv preprint arXiv:2007.11207*, 2020.
 - [53] L. Lu, P. Jin, and G. E. Karniadakis. Deeponet: Learning nonlinear operators for identifying differential equations based on the universal approximation theorem of operators. *arXiv preprint arXiv:1910.03193*, 2019.
 - [54] L. Lu, X. Meng, Z. Mao, and G. E. Karniadakis. Deepxde: A deep learning library for solving differential equations. *arXiv preprint arXiv:1907.04502*, 2019.
 - [55] T. Luo and H. Yang. Two-layer neural networks for partial differential equations: Optimization and generalization theory. *arXiv preprint arXiv:2006.15733*, 2020.
 - [56] L. Lyu, K. Wu, R. Du, and J. Chen. Enforcing exact boundary and initial conditions in the deep mixed residual method. *arXiv preprint arXiv:2008.01491*, 2020.
 - [57] M. Magill, F. Qureshi, and H. de Haan. Neural networks trained to solve differential equations learn general representations. In *Advances in Neural Information Processing Systems*, pages 4071–4081, 2018.
 - [58] Z. Mao, L. Lu, O. Marxen, T. A. Zaki, and G. E. Karniadakis. Deepm&mnet for hypersonics: Predicting the coupled flow and finite-rate chemistry behind a normal shock using neural-network approximation of operators. *arXiv preprint arXiv:2011.03349*, 2020.
 - [59] M. A. Nabian and H. Meidani. A deep neural network surrogate for high-dimensional random partial differential equations. *arXiv preprint arXiv:1806.02957*, 2018.
 - [60] Y. Nesterov. Introductory lectures on convex programming. *Lecture Notes*, pages 119–120, 1998.
 - [61] N. Nüsken and L. Richter. Solving high-dimensional hamilton–jacobi–bellman pdes using neural networks: perspectives from the theory of controlled diffusions and measures on path space. *Partial Differential Equations and Applications*, 2(4):1–48, 2021.
 - [62] G. Pang, M. D’Elia, M. Parks, and G. E. Karniadakis. npinns: nonlocal physics-informed neural networks for a parametrized nonlocal universal laplacian operator. algorithms and applications. *arXiv preprint arXiv:2004.04276*, 2020.
 - [63] G. Pang, L. Lu, and G. E. Karniadakis. fpinns: Fractional physics-informed neural networks. *SIAM Journal on Scientific Computing*, 41(4):A2603–A2626, 2019.
 - [64] P. Petersen and F. Voigtlaender. Optimal approximation of piecewise smooth functions using deep relu neural networks. *Neural Networks*, 108:296–330, 2018.
 - [65] H. Pham, X. Warin, and M. Germain. Neural networks-based backward scheme for fully nonlinear pdes. *SN Partial Differ. Equ. Appl.*, 2(1), 2021.
 - [66] A. Quarteroni and A. Valli. *Numerical approximation of partial differential equations*, volume 23. Springer Science & Business Media, 2008.

- [67] M. Raissi and G. E. Karniadakis. Machine learning of linear differential equations using gaussian processes. *arXiv preprint arXiv:1701.02440*, 2017.
- [68] M. Raissi, P. Perdikaris, and G. E. Karniadakis. Physics informed deep learning (part i): Data-driven solutions of nonlinear partial differential equations. *arXiv preprint arXiv:1711.10561*, 2017.
- [69] M. Raissi, P. Perdikaris, and G. E. Karniadakis. Physics-informed neural networks: A deep learning framework for solving forward and inverse problems involving nonlinear partial differential equations. *Journal of Computational Physics*, 378:686–707, 2019.
- [70] A. A. Ramabathiran and P. Ramachandran. Spinn: Sparse, physics-based, and partially interpretable neural networks for pdes. *Journal of Computational Physics*, 445:110600, 2021.
- [71] Y. Shin, J. Darbon, and G. E. Karniadakis. On the convergence and generalization of physics informed neural networks. *arXiv preprint arXiv:2004.01806*, 2020.
- [72] J. Sirignano and K. Spiliopoulos. Dgm: A deep learning algorithm for solving partial differential equations. *Journal of Computational Physics*, 375:1339–1364, 2018.
- [73] P. Tabuada and B. Ghahserifard. Universal approximation power of deep residual neural networks through the lens of control. *IEEE Transactions on Automatic Control*, pages 1–14, 2022.
- [74] Y. Teng, X. Zhang, Z. Wang, and L. Ju. Learning green’s functions of linear reaction-diffusion equations with application to fast numerical solver. In *Proceedings of Mathematical and Scientific Machine Learning*, volume 190 of *Proceedings of Machine Learning Research*, pages 1–16. PMLR, 15–17 Aug 2022.
- [75] J. W. Thomas. *Numerical partial differential equations: conservation laws and elliptic equations*, volume 33. Springer Science & Business Media, 2013.
- [76] J. W. Thomas. *Numerical partial differential equations: finite difference methods*, volume 22. Springer Science & Business Media, 2013.
- [77] B. Wang, W. Zhang, and W. Cai. Multi-scale deep neural network (mscalednn) methods for oscillatory stokes flows in complex domains. *arXiv preprint arXiv:2009.12729*, 2020.
- [78] C. Wang, S. Li, D. He, and L. Wang. Is l^2 physics-informed loss always suitable for training physics-informed neural network? *arXiv preprint arXiv:2206.02016*, 2022.
- [79] S. Wang, S. Sankaran, and P. Perdikaris. Respecting causality is all you need for training physics-informed neural networks. *arXiv preprint arXiv:2203.07404*, 2022.
- [80] S. Wang, H. Wang, and P. Perdikaris. Learning the solution operator of parametric partial differential equations with physics-informed deepnets. *Science advances*, 7(40):eabi8605, 2021.
- [81] G. Wen, Z. Li, K. Azizzadenesheli, A. Anandkumar, and S. M. Benson. U-fno—an enhanced fourier neural operator-based deep-learning model for multiphase flow. *Advances in Water Resources*, 163:104180, 2022.
- [82] L. Yang, D. Zhang, and G. E. Karniadakis. Physics-informed generative adversarial networks for stochastic differential equations. *SIAM Journal on Scientific Computing*, 42(1):A292–A317, 2020.
- [83] Y. Yang and P. Perdikaris. Adversarial uncertainty quantification in physics-informed neural networks. *Journal of Computational Physics*, 394:136–152, 2019.
- [84] D. Yarotsky. Error bounds for approximations with deep relu networks. *Neural Networks*, 94:103–114, 2017.
- [85] Y. Zang, G. Bao, X. Ye, and H. Zhou. Weak adversarial networks for high-dimensional partial differential equations. *Journal of Computational Physics*, page 109409, 2020.
- [86] E. Zhang, M. Yin, and G. E. Karniadakis. Physics-informed neural networks for nonhomogeneous material identification in elasticity imaging. *arXiv preprint arXiv:2009.04525*, 2020.

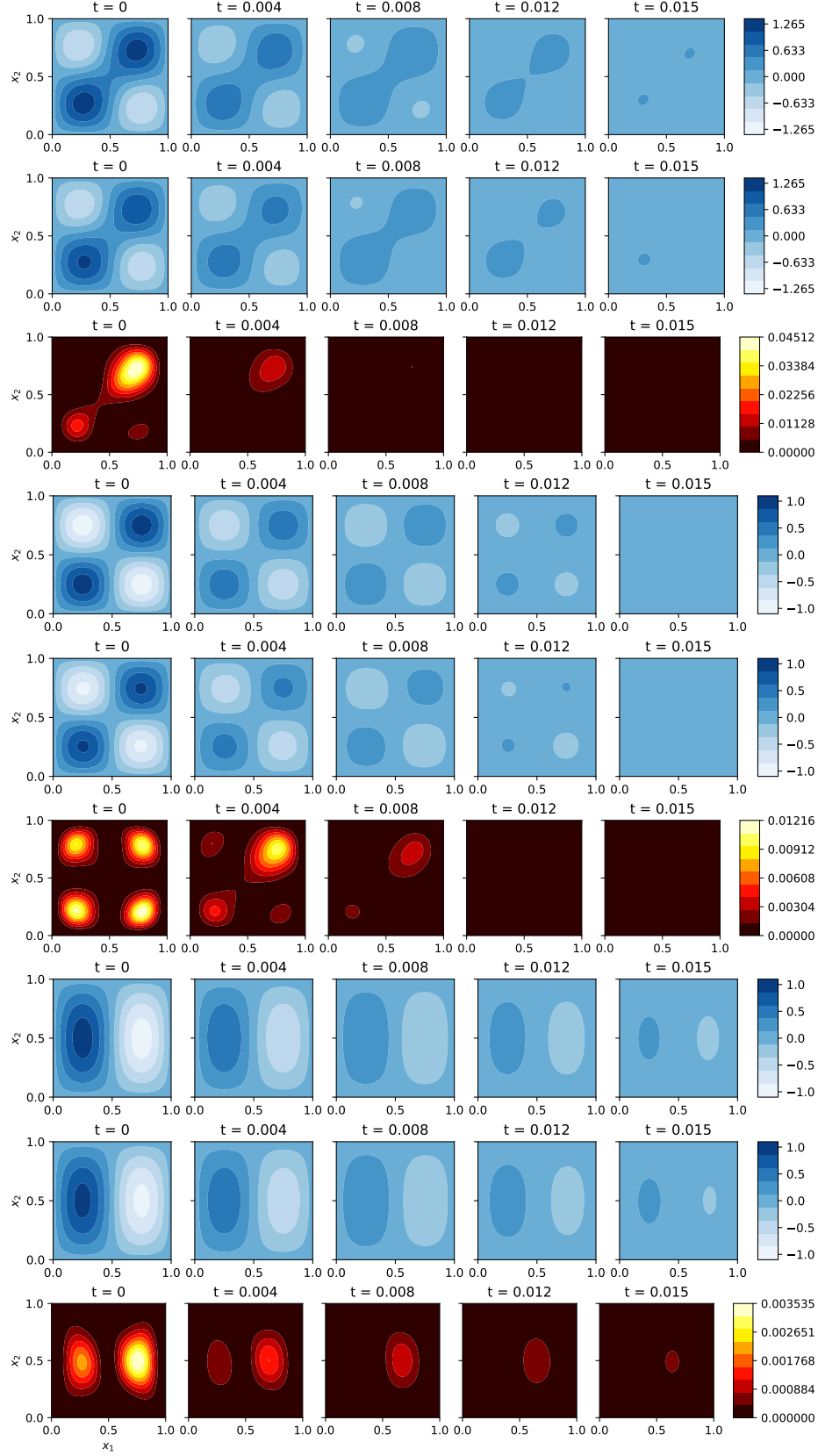


Fig. 3: (Heat equation). Comparison between true solution $u^*(\cdot, t)$, the approximation $u_{\theta_t}(\cdot)$ and their pointwise absolute difference $|u_{\theta_t}(x) - u^*(x, t)|$ for times $t = 0, 0.004, 0.008, 0.012, 0.015$ for IVPs with initial values g_1 (rows 1–3), g_2 (rows 4–6) and g_3 (rows 7–9) which are given in (4.11).

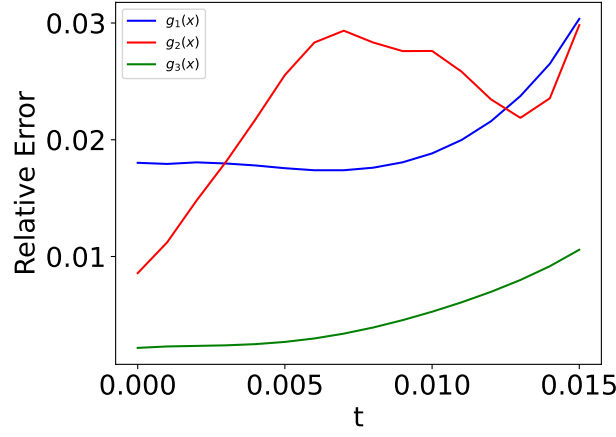


Fig. 4: (Heat equation). Comparison of the relative error $\|u^*(\cdot, t) - u_{\theta_t}(\cdot)\|_2 / \|u^*(\cdot, t)\|_2$ over time t for IVPs with initial values perturbed near g_1 , g_2 and g_3 which are given in (4.11).

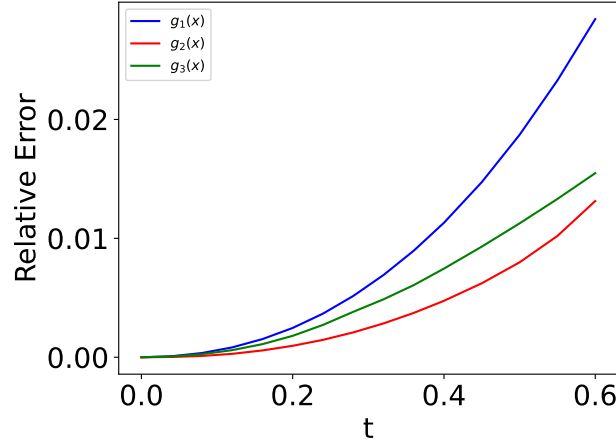


Fig. 5: (Allen-Cahn equation). Comparison of the relative error $\|u^*(\cdot, t) - u_{\theta_t}(\cdot)\|_2 / \|u^*(\cdot, t)\|_2$ over time t for IVPs with initial values g_1 , g_2 and g_3 which are given in (4.14). We notice the blow-up of the g_1 initial happens as we are closer to the development of singularities at $t = 0$ which causes the weights of u_θ to blow up.

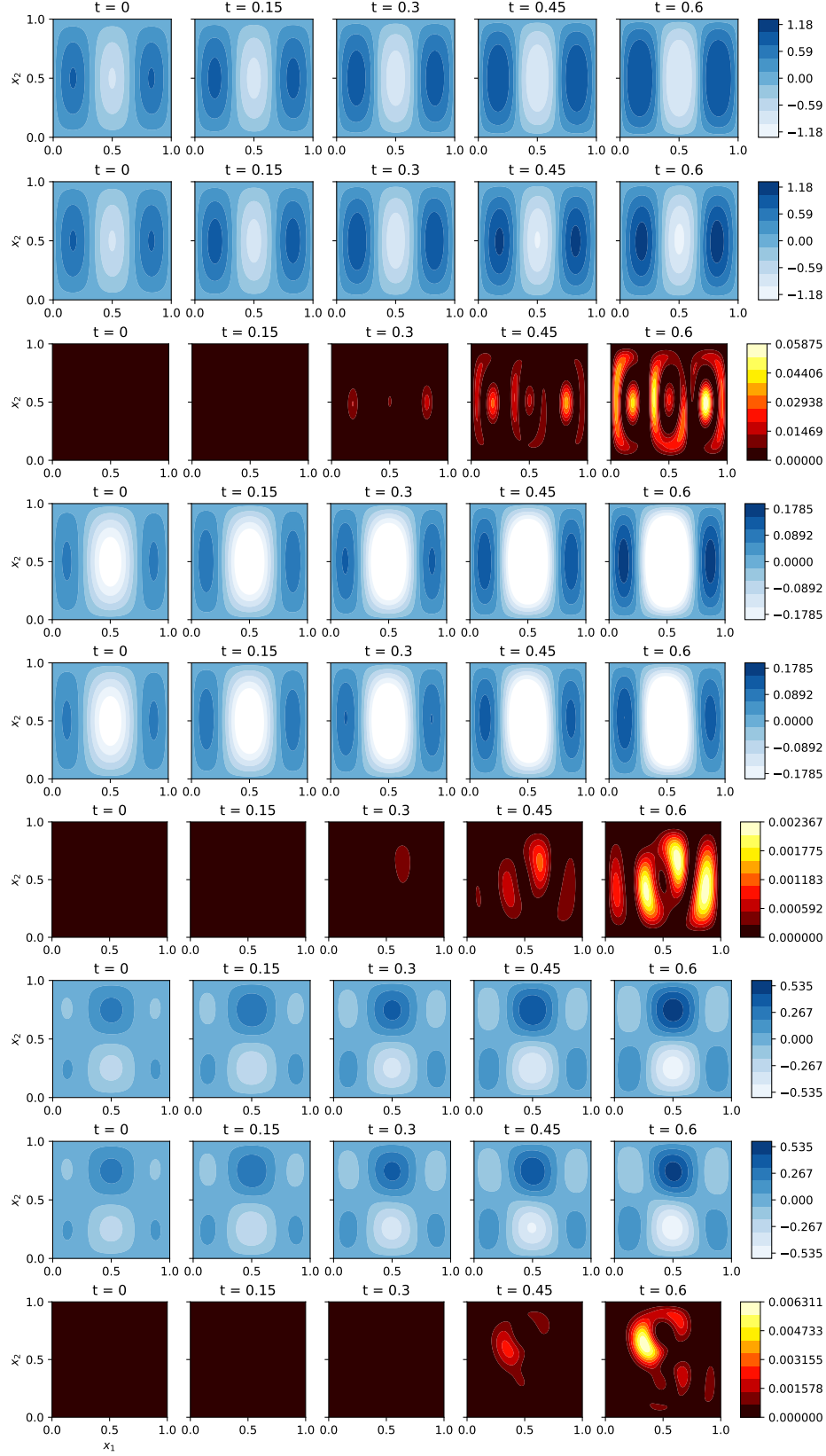


Fig. 6: (Allen-Cahn equation). Comparison between true solution $u^*(\cdot, t)$, the approximation $u_{\theta_t}(\cdot)$ and their pointwise absolute difference $|u_{\theta_t}(x) - u^*(x, t)|$ for times $t = 0, 0.15, 0.3, 0.45, 0.6$ for IVPs with initial values g_1 (rows 1–3), g_2 (rows 4–6) and g_3 (rows 7–9) which are given in (4.14).